VALIDATION OF AIRBORNE VISIBLE-INFRARED IMAGING SPECTROMETER DATA AT RAY MINE, AZ

Harold R. Lang

Jet Propulsion Laboratory, California Institute of Technology, Pasadena, CA 91109

Steve Baloga

Proxemy Research, Laytonsville, MD 20882

ABSTRACT

We validate 1997 Airborne Visible-Infared Imaging Spectrometer (AVIRIS) reflectance spectra covering 0.4 μm-2.4 μm from a stable, flat, mineralogically characterized man-made target at Ray Mine, AZ, the site for an EPA/NASA assessment of the utility of remote sensing for monitoring acid drainage from an active open pit mine. For regulatory and environmental monitoring, the "validity" of imaging spectrometer reflectance spectra is a major issue with this evolving remote sensing technology. For validation, we do three things: 1) using randomly collected field samples, we compare library, laboratory and field reflectance spectra with corresponding AVIRIS spectra; 2) using systematically collected field spectra along a ground traverse, we compare quantitatively mineralogically diagnostic statistics from field spectra with the same statistics from AVIRIS spectra; and 3) we refine the concept of "validity" and suggest a methodology for validating reflectance spectra from imaging spectrometers at active open pit mines. The fundamental promise of imaging spectrometry is to provide gridded reflectance spectra of comparable quality

as high resolution laboratory and field spectra. Results show that 1997 AVIRIS data from Ray Mine fulfill that promise, and are "valid" in this sense.

Key terms: imaging spectrometry, quantitative validation, acid mine drainage, field and laboratory spectrometry, AVIRIS, Ray Mine AZ, mineral mapping, comparative spectroscopy.

INTRODUCTION

During a five day period from January 7 through 11, 1993, 228 mm of rain (five times normal rainfall for the entire month of January) fell on Ray Mine, one of the largest active open pit mine operations in the United States. Despite controls by the mine operator to prevent leakage of hazardous material downstream from the site, this torrential rainfall event may have resulted in metal-bearing acid mine waters leaking into the Gila River, a water source for the city of Phoenix. Because of this event and ongoing water quality concerns, Ray Mine became a high priority site for monitoring by the U.S. Environmental Protection Agency (EPA). In 1997, the EPA selected Ray Mine for a demonstration project to characterize and monitor contamination from mine waste with advanced remote sensing technologies, including imaging spectrometry (EPA, 1998).

In the last decade, development of operational aircraft instruments that measure radiance from the ground in hundreds of narrow, contiguous spectral channels; the existence of libraries of reflectance spectra for minerals; development of procedures to convert aircraft radiance data to surface reflectance; and availability of commercial-off-the-shelf software to analyze spectral reflectance data on desktop computers have enabled geologists to map surface mineralogy at the resolution of

remote sensing images (typically a few m to a few tens of m). These capabilities are components of an emerging technology called imaging spectrometry.

Swayze et al. (1998) and Ferrier (1999) report imaging spectrometry results that are specifically relevant to the problem of mapping minerals that contribute to acid mine drainage from copper mining sites such as Ray Mine. They show that minerals such as jarosite, goethite, and hematite, which are formed by surface oxidation of pyrite and produce metal-rich (Pb, As, Cd, Ag, and Zn) acidic waters at mine sites, can be mapped using AVIRIS (Appendix A) data.

Although it is clear this technology potentially offers significant value for environmental monitoring, we believe that its use as a quantitative or regulatory tool first requires development of methods for validating results and interpretations. At present, even the term "validation" has yet to be clearly defined in this context.

Here we address the validation of AVIRIS reflectance data collected on April 16, 1997, over Ray Mine. We demonstrate a methodology for quantitative quality assessment of this new technology for environmental monitoring of an active open pit mine. We approach the issue of validation as one would "qualify" a new measurement method in mature traditional disciplines, such as analytic chemistry, nuclear material accountability, or nondestructive assay. Cornerstones of such qualifications include comparison of results to those obtained by other measurement methods, documentation of measurement procedures, determination of measurement reproducibility, and quantitative evaluation of sources of measurement error.

Ideally, imaging spectrometers can be used to identify and map minerals quantitatively. It is possible that such remotely-acquired data can be used to replace or supplement conventional, time-consuming, and sometimes expensive ground-sampling-based geochemistry. It could also be conjectured that imaging spectrometer data provide more representative mineralogic diagnoses because these spectral data are provided on pixel grids with resolution ranging from a few meters to a few tens of meters.

However, there are two resolution issues with such an optimistic perspective. One is the ability to resolve unique spectral features of specific minerals that may pose very different environmental concerns (jarosite versus hematite). Even in the laboratory, the difficulty of unraveling mixtures of different minerals, particle sizes, and textures is a well-known problem. The second issue is pixel size. Different mixtures of several minerals that are separable in laboratory microscopic observations or in laboratory spectra of hand samples can have the same spectrum when averaged over the thousands or millions of equivalent fields of view corresponding to a single, 20 m AVIRIS pixel.

Given these concerns and our interest in "validating" AVIRIS data, we have identified a number of specific research questions that help to focus our work:

1. Can laboratory and/or field spectral measurements of ground targets in an AVIRIS image be used to validate AVIRIS reflectance spectra after the data are acquired, or is it necessary to make field validation measurements simultaneously with an AVIRIS overflight?

2. What criteria and guidelines should be used to select a validation target at an active open pit mining site?
3. To establish the "truth" of AVIRIS reflectance spectra, is it sufficient to collect randomly a modest number of samples in the field for subsequent laboratory spectral analysis?
4. What qualitative or quantitative improvements in the validation of AVIRIS reflectance spectra result from systematic measurements along traverses or on grids with a field spectrometer?
5. What are the quantitative biases of AVIRIS reflectance spectra compared to high resolution laboratory or field spectra? Are these biases signficant and what are the major error sources? How are these considerations affected by the number of samples collected in the field?
6. Qualitatively, to what extent can AVIRIS reflectance spectra replace or supplement conventional field sampling and analyses?

These questions establish, in a practical sense, what we mean by the term "validation". In effect, our approach to answering them provides a protocol or guideline for establishing the validity (and limitations) of AVIRIS reflectance spectra for mine site monitoring.

To ensure that others can reproduce our Ray Mine results and apply our methodology elsewhere, we relied on commercial, publicly-available software and instrumentation. Appendix A is an annotated list of what we used. It includes Web addresses for accessible sources of documentation.

SITE DESCRIPTION

Ray Mine, at an average elevation of 730 m, is centered near latitude 33°N, longitude 111°E, in central southeastern Arizona (Figure 1). It is approximately 100 km north of Tucson and 100 km east of Phoenix. The town of Kearny is about 10 km SE on Highway 177. The mine is in the Mineral Creek drainage, a tributary of the Gila River.

Maps and reports documenting the geology, origin of copper deposits, and mining operations at Ray Mine include Ransome (1919), Wilson et al. (1959), Metz et al. (1968), Phillips et al. (1971 and 1974), and Creasey et al. (1983).

Primarily from Ransome (1919) and Creasey et al. (1983), Figure 2B shows the geology of the area covered by our 1997 AVIRIS data (Figure 2A). The geology east of 111°W is from Ransome's 1919-vintage map, and thus depicts surface geology prior to open pit mining.

At the base of the exposed section are the Proterozoic Pinal Schist, Madera Diorite and Ruin Granite. These rocks are overlain unconformably by Proterozoic sedimentary rocks and basalt flows of the Apache Group and Troy Quartzite, which are intruded by diabase dikes and sills. Unconformably above these rocks are Paleozoic carbonates including the Martin Limestone. Late Cretaceous through Paleocene granitic stocks and dikes of the Granite Mountain Porphyry and Teapot Mountain Porphyry intrude older rocks. Later Cenozic cover includes the Whitetail Conglomerate, dacite and rhyolite lava flows and tuffs, and coarse-grained siliciclastic and gypsiferous beds of the Gila Formation.

A major structural discontinuity coincides with Mineral Creek drainage. Excavation of the pit exposed the Diabase Fault on the east side of the drainage,

where Pinal Schist on the west abuts younger rocks on the east (Metz et al., 1968; Phillips et al., 1974).

Disseminated copper ores result primarily from hydrothermal alteration of the Pinal Schist, diabase sills, and Granite Mountain Porphyry (Metz et al., 1968). Three types of ore exist: chalcocite, chalcopyrite, and chrysocolla (Metz, 1968; Phillips et al., 1974).

Supergene-altered caprock, averaging 70 m thick, covered the main orebody prior to pit excavation (Metz et al., 1968). It is leached, iron oxide-stained, light gray-green to red, fine to medium grained, foliated, sericite (muscovite)-quartz-feldspar-Pinal Schist and hornfels.

Copper mining at Ray Mine began in 1880 (Ransome, 1919). Open pit mining started in 1952 and now affects an area of over 2300 hectares (Figure 2B) which is essentially devoid of vegetation (Figure 2A). Facilities include waste and heap leach piles, tailings and leachate solution ponds, processing plants, offices, workshops, warehouses, roads, and the pit itself. A 5.5 km long tunnel carries surface waters of Mineral Creek underground around the pit which is over 350 m deep. Ore is mined at a rate of over 250,000 tons/day.

METHODS AND APPROACH

On April 16, 1997, AVIRIS radiance data were acquired over Ray Mine (Figure 2A). These data were converted to reflectance by the JPL AVIRIS data facility. The procedure of Green et al. (1996 and Green, 1998) was used. This procedure first applies MODTRAN (Berk et al., 1989), an improved version of the LOWTRAN (Kneizys, et al., 1988) radiation transfer model, to the calibrated AVIRIS radiance

data to generate a look-up table of aerosols and water vapor. A least squares regression is then performed to fit the depth of the 0.935 μm water vapor absorption band that is recorded in the calibrated AVIRIS radiance data to equivalent band depth values in the look-up table. Using results from the water vapor retrieval, the calibrated radiance data are then inverted to surface reflectance with MODTRAN. Tahl and Schonermark (1998) show that this method accurately retrieves reflectance from cloud-free, mid-latitude imaging spectrometer radiance data.

We processed and analyzed the AVIRIS reflectance data using ENVI. Initial analysis emphasized exploratory assessment of data quality. We extracted AVIRIS reflectance spectra and compared them to library spectra, edited bad and redundant channels, created color composite (e.g., Figure 2A) and ratio images, generated preliminary mineral maps (e.g., McCubbin et al., 1998), and identified a potential ground target (Figure 3) for validating the AVIRIS reflectance data.

We found that the AVIRIS reflectance data were very noisy at wavelengths short of 0.40 μm, because of low reflectance due to iron absorption. The 1.33-1.49 μm, 1.79-2.03 μm, and 2.40-2.50 μm wavelength intervals were noisy due to absorption by atmospheric water. However, once these wavelengths were deleted, our initial qualitative assessments convinced us that the AVIRIS reflectance data were of sufficient quality to warrant thorough quantitative investigation of their validity by independant laboratory and field spectral measurements.

Next, we visited the Ray Mine on February 23-24, 1998, for a coordination meeting among EPA, the mine operators, and other project participants. The objectives were to gain familiarity with the surface expression of mining operations, the geo-

logic setting and weathering processes, and the applicability of remote sensing data to specific environmental concerns. Preliminary mineral maps from AVIRIS data were evaluated and representative field samples were collected for laboratory XRD and spectral measurements for comparison with several remote sensing data sets that were available.

We also conducted a reconnaissance field examination of a potential site for validating the AVIRIS data. The site is a topographically flat, man-made surface adjacent to areas of active mining operations (Figure 2 B, 3 and 4). It was constructed by mine operators starting in 1952 when major open pit mining operations began at Ray. Although it is fairly uniform in composition, there are several topographically distinguishable units and perhaps a dozen mappable spectral units that can be delineated in interpretations of various AVIRIS color composite images. It is made of hematite-rich, leached Pinal schist and hornfels caprock, which originally covered the pit area and was stripped away to expose the orebody. This caprock material was transported to a discard area, at the validation target, west of Highway 177. Based on its appearance on the 1964-vintage USGS Teapot Mountain 7.5 minute quadrangle, this dump site has not been modified by mining operations for over 35 years; according to the mine operator there are no plans to modify it in the future. Easily accessible by dirt road from the highway, it covers 1 X 0.5 km, in two tiers, each with planar/horizontal surfaces. The site is fenced; access is only possible through a locked gate with mine operator permission and assistance.

Thus, the caprock dump site is ideally suited for use as a validation target. It is relatively large, flat, stable, and protected from further man-made modifications.

Issues of reproducibility and temporal variations are readily addressable at this target. Compared to the complexities of areas subject to active mining operations, the surface is relatively homogenous, yet possesses enough visible and spectral heterogeneity to make a validation study at the site worthwhile. For the most part, this site is virtually free from vegetation cover and significant erosion and channeling due to rainfall. It is large enough so that spatial and statistical assessments can be performed on transects corresponding to a significant number of 20 m AVIRIS pixels. Even without GPS, transects can be located accurately in the field within about one or two AVIRIS pixels by using adjacent geomorphic and man-made features such as gullies and roads.

Therefore, we collected 24 random surface rock samples, eight each on three, 100 m long, randomly oriented traverses of the upper (western) tier of the dump for laboratoy XRD and spectral measurement. We also identified several potential lines of transect across the target for subsequent sampling with a field spectrometer.

We returned to the validation target on June 2-3, 1998, to make ASD field spectral measurements (Figure 4). Prior to going to the field, we had plotted the locations of potential lines of transect on 1:6000-scale enlargements of the AVIRIS image (e.g., Figure 3) and the Teapot Mountain quadrangle.

In the field, we located the transects on the ground. This was done by combined use of the 1:6000-scale image and map, a Trimble GPS system equipped with an OMNISTAR real-time differential measurement antenna, and standard surveying methods with Brunton compass and a 20 m measuring rope. Stations were plot-

ted on the enlarged image and map to allow identification of specific corresponding AVIRIS pixels.

All together we measured 406 ASD spectra on three transects across the target. Transect lengths ranged from 100 m to 300 m. In this paper, we report results from transect A (Figure 3 and 4); which is oriented N49°E, from longitude 111°00'30.7"W/ latitude 33°09'45.4"N (on the upper tier at 788 m elevation) to 111°00'20.3"W/ 33°09'52.8"N (lower tier, 763 m). We staked stations every 20 m on the transect which covered 140 m on the upper tier and 165 m on the lower tier. A gap of 40 m, where 30° slopes exist on the edges of the two tiers, separates the two segments.

Between 14:20 and 15:20 on June 2, we measured ASD spectra on the upper tier of the transect (Figure 3); and between 10:45 and 11:00 on June 3, on the lower tier. The sky was cloud-free when we made the measurements.

With optics providing an 8° field of view, the spectrometer head was mounted at the end of a 1 m stick to avoid measurement contamination by light reflected off the operator. Measurements were made with the head 1 m above the surface, positioned so no shadows fell on the surface in the instrument's field of view.

We followed the same procedure in acquiring two standard and 10 ground spectra at each staked station on the transect:

1. Two spectra of the Spectralon standard mounted horizontally on a tripod were measured.
2. Five spectra of the ground at random locations around the stake were measured next.

3. Five spectra of the ground at random locations around a point 3 m down the transect towards the next station were then measured.
4. We then moved the standard to the next station to begin the process again.

Two standard measurements at each station were taken to ensure that at least one good standard was available for reducing the radiance data to reflectance. Having duplicates also engenders the possibility of estimating the contribution of standard calibration errors, a topic for subsequent study. Measurement of standards at each station also minimizes systematic errors due to instrument drift and changes in solar illumination and sky conditions. Ten ground spectra were measured at each station so that statistically meaningful confidence intervals could be calculated for mean values of spectra, derived absorption band depths and band ratios, for comparison with results from other stations, AVIRIS, and laboratory spectra.

After all measurements were completed, we removed most of the stakes, but left enough labeled stakes in place to make it possible to relocate all stations. After returning from the field, we downloaded radiance and timing files from the instrument's computer onto our desktop computers for subsequent conversion to reflectance and analysis.

VALIDATION TARGET RESULTS

Analyses of Random Field Samples

Introduction — Here we summarize our assessment of the spectral characteristics of the upper tier of the target. This is based on comparing, qualitatively, results from laboratory XRD measurements and spectra of the random rock samples col-

lected in February, 1998, corresponding ASD field spectra collected in June, 1998, and corresponding AVIRIS spectra collected in April, 1997.

Spectra came from four different instruments that differ in mode of measurement (hemispherical for the Beckman and PIMA and bidirectional for the ASD and AVIRIS), field of view, spectral resolution, and method for reflectance calibration (Table 1). All four instruments provide reflectance spectra, which show changes with wavelength of the ratio of radiance off the sample surface divided by the radiance off the surface of a sample with 100 % absolute reflectance, expressed in percent.

Conversion of AVIRIS radiance data to percent reflectance was by the Green et al. (1996 and Green, 1998) method. Conversion of the radiance data from the three other instruments to reflectance was a three step process, using commercial software provided with the Beckman and PIMA instruments and Excel software for the ASD. The radiance value recorded by a particular instrument at each wavelength was treated as follows:

1. The radiance value of the sample was divided by the radiance value for the standard (halon was the standard for the Beckman; and spectralon, for the ASD).
2. The result from 1. was multiplied by 100 to obtain apparent percent reflectance.
3. The result from 2. was multiplied by a factor (available from the standard's manufacturer) that corrects for the deviation of the standard from 100 % absolute reflectance.

Mineralogy and Library Spectra — Field descriptions of the rocks and regolith and laboratory bulk sample XRD analyses of rock surfaces provided the mineralogy of the surface of the upper tier of the validation target. A Philips diffractometer was used for the XRD measurements, and standard bulk sample procedures (Brindley and Brown, 1980; Carroll, 1970; Klug and Alexander, 1954) were followed. Seven minerals were identified: quartz, kaolinite, plagioclase, jarosite, muscovite, goethite, and hematite. This mineral suite is typical of that reported for supergene-altered rocks (Sabine, 1999, p. 395-399). The spectra for these seven minerals, shown on Figure 5, were extracted from the Grove et al. (1992) spectral library. The library spectra were measured using the same Beckman spectrometer that was used to measure spectra of field samples. To make the figure, we excluded data from wavelengths short of 0.40 μm, between 1.33–1.49 μm, between 1.79–2.03 μm, and long of 2.40 μm. This was to facilitate direct comparison of these spectra to AVIRIS spectra which exhibit excessive noise over excluded wavelengths.

We assume that these seven library spectra exhibit all of the spectral characteristics for the minerals that are mixed intimately to form the surface of the validation target. The minerals are mixed intimately because they occur as clay to sand sized particles that form the clay to sand sized regolith and the pebble to cobble sized rock fragments that constitute the target surface.

Examination of the spectra in Figure 5 shows that except short of 2.03 μm where kaolinite has the highest reflectance, quartz exhibits the brightest and flattest spectrum of the seven minerals. Except short of 0.51 μm where jarosite has the lowest reflectance, hematite has the darkest and flattest spectrum. Therefore, addition

of quartz to mixtures of these minerals should increase overall reflectance; and addition of hematite, decrease overall reflectance.

Each of the seven mineral spectra has characteristic absorption bands at specific wavelengths (Table 2). By absorption bands we mean reflectance minima and concave downward points of inflection on the spectra. Reflectance peaks also exist in the spectra at wavelengths between major absorption bands (Figure 5). For these minerals, the spectroscopy literature shows that the absorption bands short of 1.60 μm are caused by the ferrous and/or ferric ion, and the absorption bands long of 1.60 μm are caused by the hydroxyl ion and/or bound water (Clark, 1999; Hunt, 1980; Lang, et al., 1990; Sabine, 1999).

Based on their number, strength, position, and shape, the absorption bands provide spectral signatures that can fingerprint uniquely each mineral in the Figure 5 suite (Table 2). This may be the case with some pure minerals, but it is not this simple when dealing with the mixtures of minerals that constitute the regolith and rocks that form the surface of the validation target. For example, mixing equal parts muscovite and jarosite will yield a spectrum without the diagnostic 2.27 μm jarosite absorption band; and spectra of mixtures containing more than 1:1 parts muscovite:jarosite exhibit a 2.27 μm reflectance peak instead of a 2.27 μm jarosite absorption band. This is because the strong 2.19 μm and 2.35 μm absorption bands and 2.27 μm reflectance peak of the muscovite spectrum fill the jarosite-diagnostic, 2.27 μm absorption band.

In a simple two component mixture, we still might be able to fingerprint jarosite based on absorption bands at 0.44 μm and 0.57 μm. Unfortunately, the vali-

dation target surface is not a mixture of jarosite and muscovite only. Figure 5 shows two spectra of more realistic multicomponent mixtures calculated from the Figure 5 library spectra. Although composed of different minerals, in different concentrations, the two spectra are identical, based on the shape, strength, position, and number of absorption bands (Table 2).

Laboratory Spectra — Results of 32 Beckman laboratory spectral measurements of the surfaces of the 24 rocks that we collected in February, 1998, are illustrated in Figure 7. Offsets in the spectra at 0.80 μm are instrumental artifacts due to an error in the intercalibration of two detectors that record radiance. The overall shape of the Figure 7 spectra is very similar to the calculated library mixture spectra in Figure 6. The Beckman spectra show the highest reflectance around 1.60 μm. Comparison of these absorption bands to those of the library spectra (Figure 5) shows that the three shortest wavelength absorption bands are due to hematite; the weak 2.10 μm band is due to muscovite; and the strong 2.20 μm band and weak band at 2.16 μm are due to kaolinite as is the 2.32 μm band.

Results of 32 PIMA laboratory spectral measurements of the same sample surfaces measured with the Beckman are illustrated in Figure 8. PIMA measurements are restricted to wavelengths long of 1.30 μm. The overall shapes of the PIMA spectra are identical to those of the Beckman spectra (Figure 7) and very similar to those of the calculated library mixture spectra (Figure 6). The PIMA spectra show the highest reflectance around 1.60 μm. The four bands long of 1.30 μm are identical to those of the Beckman spectra and similarly can be attributed to muscovite and kaolinite.

Field Spectra — Results of 60 ASD field spectral measurements on the upper tier of the validation target where the samples for laboratory analysis were collected are shown in Figure 9. Offsets in these spectra at 0.99 μm are instrument artifacts due to an error in the intercalibration of two detectors that record radiance. The overall shapes of the field spectra are identical to those from the PIMA (Figure 8) and Beckman (Figure 7) laboratory instruments, and very similar to those of the calculated library mixture spectra (Figure 6). The field spectra show the highest reflectance around 1.60 μm. Except for the absence of a band at 2.16 μm, the absorption bands are identical to those of the Beckman and PIMA laboratory spectra. Comparison to the library mineral spectra (Figure 5) shows that the three short wavelength bands are due to hematite, and the three long wavelength bands are due to muscovite and/or kaolinite, with the weak 2.16 μm kaolinite band missing because of insufficient spectral resolution and/or dilution of the band because of mixing of the other spectral components (i.e., minerals) that form the measured surface. But a weak 2.16 μm absorption band is still expressed by asymmetry of the 2.20 μm band.

AVIRIS Spectra — Results of six AVIRIS spectral measurements on the upper tier of the validation target where samples for laboratory and upper tier field spectral measurement were collected are shown in Figure 10. The overall shapes of the image spectra are identical to those from the laboratory and field instruments, and very similar to those of the calculated library mixture spectra. The AVIRIS spectra also show the highest reflectance around 1.60 μm. As was seen in the field spectra, except for the absence of a weak band at 2.16 μm which again is only expressed by asymmetry of the 2.20 μm band, the bands seen in the AVIRIS spectra are identical

of those obtained in the laboratory. Also, as was seen with the field spectra, comparison to the library mineral spectra shows that the three short wavelength bands are due to hematite and the three long wavelength bands are due to muscovite and/or kaolinite.

Discussion — Qualitatively, all of these results agree. The Beckman and Pima laboratory, ASD field, and AVIRIS image reflectance spectra from the random samples of the upper target tier all exhibit the same absorption bands. Relatively strong absorption bands are ubiquitous at four different wavelengths: 1) 0.48-0.53 μm; 2) 0.87-0.92 um; 3) 2.19-2.20 μm; and 4) 2.32-2.35 μm (Table 2). The wings of these absorption bands create reflectance peaks at three different wavelengths near: 1) 0.78 μm; 2) 1.60 μm; and 3) 2.27 μm (Figures 7, 8, 9 and 10; Table 3). Relatively weak absorption bands are at 0.65-0.67 μm and 2.10 μm (Table 2). Another weak band at 2.16 μm, which is resolved in the Beckman and Pima laboratory spectra, is expressed by the asymmetry of the major 2.19-2.20 μm band in the ASD field and AVIRIS image spectra.

These absorption bands and reflectance peaks provide diagnostic spectral signatures for the seven minerals that are mixed intimately to form the surface of the validation target (Figure 5 and Table 2). However, some relatively weak but diagnostic mineral absorption bands that appear in library spectra do not exist in the field and image spectra. These include bands at 0.41 μm (due to goethite); 0.44 μm, 0.57 μm, and 2.27 μm (jarosite); 0.96 μm, 1.23 μm, 1.30 μm and 2.38 μm (kaolinite); and 1.27 μm (plagioclase). These bands may be absent because of dilution due to mixing and/or because of insufficient spectral resolution by the spectrometers that we used

(Table 1). A clear example of dilution exists in reflectance spectra of mixtures of muscovite (M) and jarosite (J). If the M:J ratio of a sample exceeds 1:1, the M reflectance peak at 2.27 μm fills the J absorption band at the same wavelength. This results in a reflectance spectrum for the mixture with the 2.27 μm reflectance peak diagnostic of M but without the 2.27 μm absorption band diagnostic of J. All of our sample spectra exhibit this dilution effect.

Some systematic differences in reflectance may exist among the Beckman, Pima, ASD and AVIRIS spectra. For example, the AVIRIS spectra tend to be brighter than the laboratory spectra (compare Figure 7, 8, 9 and 10). But comparison of mean reflectances and 1 sigma values at the three wavelengths of peak reflectance show that the reflectance values of all measurement sets in fact overlap (Table 3). The 1 sigma values reflect both target spectral variability and the accuracy of the reflectance measurements. According to Green et al. (1996), agreement between AVIRIS reflectance spectra and corresponding ASD reflectance spectra is imperfect. They suggest that the differences in reflectance, which should equate to 2-4% reflectance for our spectra, is a measure of the accuracy of their method for converting AVIRIS radiance to reflectance.

Analysis of ASD Field and AVIRIS Image Spectra from Traverse A

Introduction — The addition of systematic sampling along a traverse or a grid provides a new dimension in the type of statistical comparisons that can be performed, namely analyses involving spatial correlations, trends, and other systematic changes in the spectral features. We performed a wide variety of statistical tests on the ASD spectra and how they compare quantitatively to AVIRIS spectra. For this

paper, we chose a few simple statistics measured on the ASD field and AVIRIS image reflectance spectra to capture variability of spectral bands that are mineralogically diagnostic. Specifically we used wavelength ratios, depths, and absorption slope ratios. These statistics were selected based on what we saw in our qualitative assessment of upper tier laboratory, field and image spectra. In addition, these statistics have been used previously to determine mineral abundances with spectral data (Clark, 1999; Ferrier, 1999; Mustard and Sunshine, 1999). An example of AVIRIS and ASD values for one of these statistics for stations on the traverse is shown on Figure 11.

Qualitative Comparison of Diagnostic Absorption Bands — Figures 12-18 show the mean values of the ASD spectra compared to the AVIRIS spectra for selected stations. These were selected because they produced a maximum or a minimum in one or more of the statistics from the ASD mean spectra. We also show 2-sigma limits on the ASD means as a measure of variability.

Qualitatively, the ASD mean spectra and the AVIRIS spectra are very similar in appearance, but as we noted for laboratory measurements, AVIRIS spectra are usually brighter. The degree of difference is both wavelength dependent and station dependent. Generally, the two types of spectra show relatively small differences (typically a few percent) short of 0.9 μm. They are relatively close again at the 2.20 μm absorption band. The absolute reflectance difference between these two types of spectra can be as high as 25% at the 1.60 μm reflectance peak. ASD and AVIRIS spectra for Stations 5 (Figure 15) and 15 (Figure 18) agree best over all wavelengths. The ASD and AVIRIS spectra for Station 5 differ only by a few percent.

The mean ASD spectra and AVIRIS spectra all show the same major bands at 0.86 μm and 2.20 μm that are diagnostic of mineralogy. In all spectra, the band near 2.20 μm is coincident based on visual inspection. At slightly longer wavelengths, there is a reflectance peak that exists in all spectra. In many spectra short of the 2.20 μm absorption band, a weaker, secondary band exists. Secondary bands are more evident in the ASD spectra, but usually, also appear in the AVIRIS spectra.

The location and shape of the 0.86 μm band is often slightly different when mean ASD and AVIRIS spectra are compared. In most cases, in ASD spectra the band appears rounder at the bottom and is shifted to slightly longer wavelengths. The 0.73 μm reflectance peak is plainly evident in both data sets. Around 0.65 μm, the ASD mean spectra have a weak peak at all measurement stations. Although more subdued, this peak can be detected in the AVIRIS spectra.

Quantitative Analysis of Band Ratios and Band Depths — Data acquisition and analysis has been structured to permit a direct statistical comparison of AVIRIS and ASD spectra on a station-by-station basis across the entire traverse. For statistical analyses, we used the same band depth/ratio values from AVIRIS and ASD spectra. This enabled us to obtain calibrated mean values and bound the variability with meaningful statistical confidence limits. Here we report results from the analysis of 151 ASD reflectance spectra at 15 field measurement stations that correspond to 15 AVIRIS reflectance spectra for pixels on transect A (Figure 3). AVIRIS and ASD spectra are compared at both the station-level and based on the systematic behavior along the transect.

Band ratios were calculated using the equation,

$$BR_L = \frac{R_L}{R_U} \quad (1)$$

where R denotes the reflectance and the subscripts L and U indicate wavelength. Usually L is chosen where an anticipated absorption band has a minimum (Table 2) and U is chosen at a convenient nearby reflectance peak (Table 3).

We also calculated absorption band depth using the equation:

$$BD_L = 1 - \left(\frac{R_U - R_L}{R_U + R_L} \right) \quad (2)$$

This statistic estimates the area under the reflectance spectrum removed by the absorption band between wavelengths U and L. In the cases analyzed below, U and L were the same as those used for band ratios to afford comparison of the statistical properties of (1) and (2). The same spectral data is used in both equations, so statistical inferences are identical in both cases. Alternatively, one can recast (2) in terms of the band ratio (1). Because the variability in the data enters in a different way between (1) and (2), the statistics will have slightly different performance characteristics, but any statistical inferences remain the same.

We used one other statistic, an absorption band slope ratio (ASR) calculated by:

$$ASR_{L_1L_2} = \frac{U - L_2}{U - L_1} \left(\frac{R_U - R_{L_1}}{R_U - R_{L_2}} \right) \quad (3)$$

The purpose of this statistic is to see if additional information or insight is obtained by looking at two wavelengths along an absorption band compared to the information obtained by (1) and (2). Both AVIRIS and ASD spectra show weak absorption

bands superimposed on more prominent bands (e.g., the weak kaolinite band at 2.16 μm on the 2.20 μm band). The statistic from (3) compares the ratios of the decreases per interval at the locations of major and secondary absorption bands.

Statistical Analysis — Standard 95% confidence intervals were computed for the means of these statistics for ASD spectra from each station. The significance of the bias was determined by the location of the AVIRIS value relative to the confidence interval on the mean ASD spectrum. Those AVIRIS values within the confidence interval of the ASD means were considered statistically insignificant.

The magnitudes of the biases between the ASD means and AVIRIS spectra are very modest, typically a few percent and in some cases less. The exceptions were statistics based on the 2.16 μm and 2.20 μm data, jointly. These biases ranged as high as several tens of percentages at the station level.

For all band ratios, depths, and the ASR, the preponderance of biases were significant at the station level. Typically only three or four of the 15 measurement stations' biases from the AVIRIS values were insignificant. Most biases were positive, indicating that AVIRIS values were smaller. This is expected from our construction of band ratio and the overall higher reflectance of AVIRIS spectra compared to ASD spectra. Only the statistics from equation (3), based on the 2.16 μm and 2.20 μm data jointly, had a negative bias.

Table 4 summarizes descriptive statistics for the band ratios, band depths, and ASRs computed from the ASD mean and the corresponding AVIRIS spectra. The first column shows the mean value of all 15 AVIRIS/ASD relative biases along the transect. In all cases, the band depth algorithm provides significantly smaller biases

than the band ratio algorithm due to the way it is calculated from the data. It should be recalled, however, that the statistical significance of the bias is unaltered by the choice of the algorithm.

The second and third columns compare the standard deviations on a relative percent basis. The most commonly used statistic for such a comparison is the relative standard deviation (RSD), i.e., the conventional sample standard deviation divided by the average. As is commonly done to compare the variability of different data sets, we express this as a percentage (RSD% = RSD x 100).

The field data column represents the standard deviation based on the ASD mean values at the 15 stations. The RSD% based on ASD data pooled for all measurement stations (not shown in Table) ranges from slightly higher to about a factor of two higher. In all cases, the band depth algorithm provides less dispersion for both AVIRIS and ASD spectra. We expect this because the band depth algorithm compresses the absorption band into a tighter range than the band ratio algorithm.

A visual inspection of these two columns shows that the dispersion of the station means along the transect is comparable to the dispersion detected by AVIRIS, which is lower by about a factor of two. This comparability is an important part of the selection of the validation target. First, it means the target is sufficiently homogeneous and spectrally (mineralogically) well-behaved at the scale sampled by the field measurements. A less constrained surface might easily have an RSD field value well in excess of 100%. This would be equivalent to a low signal-to-noise ratio in the behavior of the band ratios or depths along the transect, making comparisons of ASD spectra with AVIRIS spectra a difficult proposition. Second, a comparison of

these two columns suggests that any significant systematic spatial variations along the transect are capable of being detected by AVIRIS and validated by the ASD field spectral measurements. At best, this would be difficult to assert without the availability of field measurement along a spatial traverse and modest, constrained mineralogic variations.

We have qualitatively investigated possible systematic behavior along the transect by visual comparison of the ASD and AVIRIS values for all of the absorption statistics. Specifically, we looked for systematic increases or decreases and shifts in the mean. The results are summarized in Table 5. Although variability is present in almost every case, some form of systematic behavior was identified unambiguously in all charts except for those with band ratios and depths using 2.20 μm reflectance.

There are many ways to quantitavely test for various kinds of systematic behaviors in data along a traverse or grid. For this first-order level of analysis we chose the standard correlation coefficient, more properly known as the Pearson product moment coefficient. This elementary descriptive statistic measures the statistical relationship between the value of the band depth and the distance along the traverse. Correlation coefficients of plus and minus 1 indicate perfect positive and negative linear correlations with zero indicating that band depth and distance are statistically independent. It is beyond the scope of this analysis to consider measures of nonlinear correlation. One could also approach the detection of systematic behavior along the transect from a regression perspective. However, the most common sta-

tistical measure of "goodness of fit", the "r-squared" is ultimately related to the Pearson product moment coefficient.

The band ratio and the distance along the transect were taken as the variables, separately, for the ASD means and the values from AVIRIS. The computed correlation coefficients appear in the third and fourth columns. Note how well these correspond to the visual impressions of systematic behavior in Figures 11 through 18.

The test statistic for evaluating the difference between two Pearson coefficients is given by

$$Z = \frac{Z_1 - Z_2}{\sqrt{\frac{1}{n_1 - 3} - \frac{1}{n_2 - 3}}} \tag{4}$$

where

$$Z_i = \frac{1}{2} \ln\left(\frac{1 + r_i}{1 - r_i}\right) \tag{5}$$

is the Fisher transformation of the Pearson coefficient, r_i. This transformation makes Z a normally distributed random variable, whose statistical significance is easy to evaluate. Thus, differences in two Pearson coefficients are considered insignificant when the test statistic is within the critical region (-1.96, 1.96) at the standard 0.05 level of significance.

The values of the test statistic are shown in Table 5. Given that we have only 15 measurement stations, the results are striking. In no case, is the test statistic outside the critical region or even approaching a significant difference. When system-

atic behavior in band ratio, band depth, or ASR was detected along the transect by the ASD measurements, systematic behavior was also detected by AVIRIS.

It is tempting to push the comparability further by regressing ASD values directly on the AVIRIS values from equations (1), (2), and (3). Due to the natural variability along the transect, however, this is asking too much. In all cases, the regressions were found to be statistically insignificant or dominated by numerous locations with "lack of fit". Stated another way, there is too much natural variability in the surface, probably attributable to subtle compositional changes, to make regression meaningful in a statistical sense. Stated yet another way, these data cannot be interpreted as being derived from a system in a state of statistical control, as one encounters in a typical calibration problem. This means that the ASD band ratios vary in a way that cannot be predicted from the corresponding AVIRIS values, nor could a set of band ratios be used by "inverse calibration" methods to predict uniquely the AVIRIS band ratio values.

Discussion — Part of the issue of "validity" is whether the compositionally diagnostic spectral features observed in AVIRIS reflectance spectra are the same as those found in field spectra. Our ASD field spectra show, measurement station by measurement station, that the key diagnostic features are present in both data sets. Moreover, the wavelengths and magnitudes of absorption bands and reflectance peaks correspond sufficiently well that the AVIRIS spectra can be considered "validated". By this we mean that AVIRIS reflectance spectra deliver the same compositional information that the ASD spectra provide. However, there is generally a difference between ASD and AVIRIS spectra in albedo that is a function of

wavelength. Moreover, the shapes of the absorption features can be slightly different. For example, the mean ASD spectra have a rounder and often broader 0.86 μm absorption band. Although "validated" in the sense above, band ratios or band depths computed from AVIRIS spectra can be significantly biased which might lead to inaccurate quantitative mineral identifications compared to laboratory or field spectra of multimineralic mixtures.

These results apply to this particular 1997 AVIRIS reflectance data set only. Assessment of AVIRIS system stability over time is not addressed. But validating AVIRIS data acquired subsequently, including a 1999 dataset with 5 m spatial resolution, should be possible using the same field spectra that were acquired in this study.

SUMMARY AND CONCLUSIONS

AVIRIS spectra are thought to contain signatures of minerals that could pose an environmental concern for nearby water sources. We compared spectral features found in the 1997 AVIRIS reflectance spectra for the Ray Mine site with laboratory and field spectra of randomly and systematically collected ground samples. The fundamental promise of imaging spectrometry is to provide gridded reflectance spectra of the comparable quality as high resolution laboratory and field spectra. Results show that the 1997 AVIRIS data from Ray Mine fulfill that promise, and are "valid" in this sense. Here we amplify our fundamental conclusion in four areas: 1) comparisons obtained by random sampling; 2) comparisons obtained by systematic sampling; 3) general guidelines concerning the interpretation of the term "validation" for such a site; and 4) generalizations of the methodology we used.

Conclusions Related to Random Sampling of the Field Site

Qualitatively, Beckman and Pima laboratory, ASD field and AVIRIS image reflectance spectra all exhibit the same absorption bands. Relatively strong absorption bands are ubiquitous at four different wavelengths: 1) 0.48-0.53 μm; 2) 0.87-0.92 μm; 3) 2.19-2.20 μm; and 4) 2.32-2.35 μm. The wings of these absorption bands create reflectance peaks at three different wavelengths near: 1) 0.78 μm; 2) 1.60 μm; and 3) 2.27 μm. Relatively weak absorption bands are at 0.65-0.67 μm and 2.10 μm. Another weak band at 2.16 μm is resolved in the Beckman and Pima laboratory spectra, but is only expressed by the asymmetry of a major 2.19-2.20 μm band in ASD and AVIRIS spectra.

These absorption bands and reflectance peaks provide diagnostic spectral signatures for minerals that are mixed intimately to form the surface of the validation target. However, some relatively weak but diagnostic mineral absorption bands that appear in library spectra do not exist in ASD and AVIRIS spectra. These include bands at 0.4 1 μm (due to goethite); 0.44 μm, 0.57 μm, and 2.27 μm (jarosite); 0.96 μm, 1.23 μm, 1.30 μm and 2.38 μm (kaolinite); and 1.27 μm (plagioclase). These bands may be absent because of dilution due to mixing and/or because of insufficient spectral resolution by the ASD and AVIRIS spectrometers. A clear example of dilution exists in reflectance spectra of mixtures of muscovite (M) and jarosite (J).

Some systematic differences in reflectance exist among the Beckman, Pima, ASD and AVIRIS spectra. AVIRIS spectra tend to be brighter than the laboratory spectra, but comparison of mean reflectances and 1 sigma values at the three wavelengths of peak reflectances show that the reflectance values of all measurement sets overlap. The 1 sigma values reflect both target spectral variability and the accuracy

of the reflectance measurements. These differences in reflectance are a measure of the accuracy of AVIRIS reflectance derived from calibrated AVIRIS radiance.

Qualitative comparison of the library and Beckman spectra from field samples suggests that the three shortest wavelength absorption bands are due to hematite; the weak 2.10 μm band is due to muscovite; and the strong 2.20 μm band and weak band at 2.16 μm are due to kaolinite as is the 2.32 μm band. Similar conclusions hold for Pima spectra which only cover wavelengths beyond 1.3 μm. Qualitative comparison of AVIRIS spectra to library spectra suggests that the three short wavelength bands are due to hematite and the three long wavelength bands are due to muscovite and/or kaolinite. A weak 2.16 μm kaolinite band may be missing in AVIRIS spectra due to dilution caused by mixtures of several minerals in the measured surface. Thus, qualitatively the laboratory, field and AVIRIS spectra provide identical mineralogical information.

Field descriptions of the rocks and regolith at the validation target, and laboratory XRD analyses of the randomly collected samples, unambiguously indicates the presence of seven minerals: quartz, kaolinite, plagioclase, jarosite, muscovite, goethite, and hematite. Calculated mixtures of library spectra for these minerals reproduce spectral features observed in the AVIRIS data. However, because of the intimate mixing of these minerals in the natural setting of validation target rocks and regolith, a complete, unique and quantitative mineralogical decomposition starting with an AVIRIS reflectance spectrum is not possible.

Conclusions Related to Systematic Sampling of the Field Site

In general, the agreement between AVIRIS and ASD field spectra is remarkably good. Band ratios and band depths from AVIRIS spectra tend to be systematically and significantly biased low from mean ASD values. Typically, this bias is 5% or less and it is present on a station-by-station basis and for all data across the transect. In some cases, however, the bias is randomly distributed about the ASD mean values. When a spatial trend on the order of 5-10% is present in ASD data across the transect, AVIRIS data tends to detect it, particularly at lower wavelengths.

Band ratio and band depth statistics provide approximately the same systematic spectral information across a transect of a few hundred meters in length. However, the statistical performance of band depth in estimating mean statistical properties is slightly preferable.

Conclusions Concerning "Validation"

Imaging spectrometer data such as that provided by AVIRIS are not likely to be accepted for detecting, mapping or monitoring minerals or compounds of environmental concern until the "validity" of the data has been established. From a practical standpoint, for use in formal environmental projects by the USEPA, imaging spectrometer data must be validated and a formal definition of what validation means must exist.

Based on our results, we propose a preliminary working definition of "validation" of imaging spectrometer data for environmental monitoring:

> "Validation of imaging spectrometer data means that the spectral features of interest have been verified by independent measurement methods of sufficient accuracy and precision, and traceable to national standards, to

answer specific questions of environmental concern, with adequate levels of confidence under similar measurement conditions. Enough independent samples must be measured to assure that extrapolations are representative of AVIRIS image spectra."

We suggest that future research should attempt to use and refine this definition. Ultimately, a formal definition must be established and accepted by the regulator-regulatee-data provider community. Clearly issues such as the calibration of AVIRIS, field and laboratory spectrometers data are embraced by this working definition under the statement regarding accuracy. The key point, however, is that a specific question or issue must be posed to make the practical definition of "validity" meaningful.

For example, if we are interested in determining only whether or not iron or hydroxyl absorption bands detected in AVIRIS spectra are present at the surface, then a few random samples for laboratory analysis or field spectrometry may only be necessary to establish validity. We find that laboratory measurements of a relatively small collection of field specimens is probably adequate, and little information relevant to validation is gained by devising field spectral surveys requiring large resources. If sufficient a priori information about the mineralogy of a representative target exists, then library spectra may be adequate even without field specimens.

On the other hand, if we are interested in the quantitative validation of band depths or band ratios across large surface areas, then combinations of systematic and random sampling are necessary to establish biases, statistical confidence intervals, and estimate the representativeness of the ground measurements. Finally, if we are

interested in validating interpretations of AVIRIS spectra aimed at identifying specific minerals, then laboratory analyses are required to confirm unambiquously mineral identifications and how mineralogy varies over an AVIRIS scene.

An important theme of imaging spectroscopy research has been development of algorithms that use library spectra as a basis for analyzing image spectra to identify minerals and mineral mixtures using spectral criteria. Pixel-by-pixel mineral/mineral mixture identifications are then used to create maps of surface mineralogy. Criteria used include the wavelengths of absorption bands and reflectance peaks, depths of absorption bands, and absorption band shapes from library or field spectra.

We find that mapping algorithms that incorporate information regarding spectral absorption band shapes might not be the best or most efficient approach to material identification, because band shape is affected greatly by variations of absolute reflectance. Instead, especially when one considers that for targets such as ours, only a few (fewer than seven, Table 2) diagnostic spectral absorption features seem to describe adequately all of our laboratory, field and image spectra, a few band ratios may be adequate and appropriate parameters for identifying all minerals that are detectable spectrally.

Mapping algorithms all rely on the assumption, often unstated and unvalidated quantitatively, that reflectance spectra from imaging spectrometers are equivalent in quality to library or field spectra. Our results validate this assumption for 1997 AVIRIS reflectance spectra from Ray Mine. Because AVIRIS wavelength and radiance calibration is carefully validated yearly in the laboratory and in flight (e.g., Green et al., 1998) and improves every year, this conclusion should be applicable to

AVIRIS data acquired since 1997 provided the calibrated radiance data are amenable to conversion to reflectance using the Green et al. (1996 and Green, 1998) method.

The representativeness of ground measurements must also be considered for validation over large areas. It would be easy at the Ray Mine site to repeatedly sample centimeter scale fields of views with a field spectrometer until one found a spectrum identical to a corresponding AVIRIS or library spectrum. This however is exploration, rather than validation, and has no bearing on representativeness.

We believe that the methodology that we used over our validation target is a practical alternative to the random nested sampling procedure that is commonly used for validating remote sensing results. If we assume that under clear sky conditions the sensor is stable during the short time (<2 minutes) required to collect the Ray Mine AVIRIS scene (Figure 2A), and that atmospheric conditions throughout the small area (250 km^2) are constant and well characterized in the MODTRAN reduction to reflectance, than validation results from a single validation target such as ours should be applicable over the rest of the scene.

The caprock dump is an ideal validation target at Ray Mine. More importantly caprock dumps are commonly created in the early phase of open pit mining. Thus, they exist at many open pit mining sites and could serve as validation targets elsewhere.

Conclusions Concerning the Methodology and Possibilities for Generalization

Our multifaceted approach permits us to make precise statements regarding the "validity" of AVIRIS data. It is likely that this approach can be generalized to other

ground validations of AVIRIS reflectance data sets acquired for environmental assessment.

Our methodology, using commercial software and instruments, could be adopted as a standard operating procedure (SOP) for validating imaging spectrometer data for monitoring active mine sites of interest to the USEPA. Five steps are required:

1. Posing a well-defined issue that is to be validated (e.g., the validity of a specific spectral feature qualitatively in the AVIRIS data, the validity of a band ratio quantitatively, or the detection of the quantitative abundance of a specific mineral or suite of minerals);
2. Definition of the validation target under consideration (for example, the caprock dump target at Ray Mine);
3. Field investigation of the validation target to assess homogeneity, vegetation, and other properties such as slopes that affect AVIRIS measurements;
4. Design of a sampling and analysis plan that can establish "validity" at the appropriate level of detail; and
5. Analysis of data, establishment of conclusions, and, most importantly, determining the limitations of the validation statements.

We have found that this approach defines and establishes "validity" of AVIRIS reflectance spectra at a number of different levels for the Ray Mine site. It is likely that this approach can be applied to other active open pit mines that may pose environmental concerns.

ACKNOWLEDGMENTS

This paper presents results of research carried out at Jet Propulsion Laboratory, California Institute of Technology, and Proxemy, Inc., under contract with the National Aeronautics and Space Administration (NASA). Tom Mace, USEPA, is PI for the project. Our work would not have been possible without the generous help of ASARCO personnel, particularly Neil Gambell who provided geological information and facilitated our activities at the mine, Larry Hagy who helped us in the field in February, 1998, and Ed Meza who arranged access in June, 1998. John Hillenbrand provided background information about the site. Rob Green developed the software and reduced the 1997 AVIRIS data to reflectance. Betina Pavri taught us how to use the ASD spectrometer and helped us use the instrument in the field. Marty Grove provided access to the x-ray diffractometer facility in the Department of Earth and Space Sciences, UCLA. Cindy Grove made the XRD mineralogical determinations and measured Beckman and PIMA spectra in the laboratory. Assistance from Lori Glaze on ASD measurements and Bruce Campbell on spectral analysis is greatly appreciated. An early draft of the paper benefited from constructive comments from Tom Mace and Mike Abrams. Reference herein to any specific commercial product, process, or service by trade name, trademark, manufacturer, or otherwise does not constitute or imply endorsement by NASA, the United States government or Jet Propulsion Laboratory, California Institute of Technology.

REFERENCES CITED

Brindley, G.W., and Brown, G., eds., 1980, Crystal structures of clay minerals and their X-ray identification: London, Mineralogical Society Monograph 5, 495 p.

Berk, A., Bernstein, L.S., and Robertson, D.C., 1989, MODTRAN: a moderate resolution model for LOWTRAN7: Air Force Geophysics Laboratory, Hanscom AFB, MA, GL-TR-89-0122, 38 p.

Clark, R.N., 1999, Spectroscopy of rocks and minerals and principles of spectroscopy, in, Rencz, A.N., ed., Remote Sensing for the Earth Sciences: Manual of Remote Sensing, 3 ed., v. 3, New York, John Wiley, p. 3-58.

Carroll, D., 1970, Clay minerals: a guide to their X-ray identification: GSA Special Paper 126, 80 p.

Creasey, S.C., Peterson, D.W., and Gambell, N.A., 1983, Geologic map, Teapot Mountain Quad, Arizona: USGS, Map GQ-1559, 1:24,000-scale geologic map with explanatory text.

EPA, 1998, Advanced measurement initiative workshop report: advanced measurement and site characterization of mining impacts on public health and the environment, July 14-17, 1997, Colorado School of Mines, Golden, Colorado: United States Environmental Protection Agency, Office of Policy, EPA-235-R-98-002, 22 p.

Ferrier, G., 1999, Application of imaging spectrometer data in identifying environmental pollution caused by mining at Rodaquilar, Spain: Remote Sensing Environment, v. 68, p. 125-137.

Grove, C.I., Hook, S.J., and Paylor, E.D., II, 1992, Laboratory reflectance spectra of 160 minerals, 0.4 to 2.5 μm: JPL Publication 92-2, 26 p. and 3 appendices.

Green, R.O., 1998, Apparent surface reflectance of the DOE ARM SGP CART central site derived from AVIRIS spectral images: Summaries of the Seventh JPL Earth Science Workshop, JPL Pub. 97-21, v. 1, p. 175-184.

Green, R.O., Pavri, B., Faust, J., Williams, O., Chovit, C., 1998, Inflight validation of AVIRIS calibration in 1996 and 1997: Summaries of the Seventh JPL Airborne Earth Science Workshop, JPL Pub. 97-21, v. 1, p. 193-203.

Green, R.O., Roberts, D.A., and Conel, J.E., 1996, Characterization and compensation of the atmosphere for inversion of AVIRIS calibrated radiance to apparent surface reflectance: Summaries of the Sixth Annual JPL Airborne Earth Science Workshop, JPL Pub. 96-4, v.1, p. 135-146.

Hunt, G.R., 1980, Electromagnetic radiation: the communication link in remote sensing, in Siegal, B.S., and Gillespie, A.R., eds., Remote Sensing in Geology: New York, John Wiley, p. 5-45.

Klug, H.P., and Alexander, L.E., 1954, X-ray diffraction procedures: New York, Wiley, 716 p.

Kneizys, F.X., Shettle, E.P., Abreu, L.W., Chetwynd, J.H., Anderson, G.P., Gallery, W.O., Selby, J.E.A., and Clough, S.A., 1988, User's guide to LOWTRAN 7: Air Force Geophysics Laboratory, Hanscom AFB, MA, AFGL-TR88-0177, 137 p.

Lang, H.R., Bartholomew, M.J., Grove, C.I., and Paylor, E.D., 1990, Spectral reflectance characterization (0.4 to 2.5 and 8.0 to 12.0 μm) of Phanerozoic strata, Wind River basin and southern Bighorn basin areas, Wyoming: Journal of Sedimentary Petrology, v. 60, n. 4, p. 504-524.

McCubbin, I., Lang, H., Green, R.O., and Roberts, D., 1998, Mineral mapping using AVIRIS data at Ray Mine, AZ: Summaries of the Seventh JPL Airborne Earth Science Workshop, JPL Pub. 97-21, v. 1, p. 269-272.

Metz, R.A., Phillips, C.H., and Caviness, C.R., 1968, Recent developments in the geology of the Ray area: in, Titley, S.R., ed., Arizona Geological Society, Southern Arizona Guidebook III, p. 137-146.

Mustard, J.F., and Sunshine, J.M., 1999, Chapter 5, Spectal analysis for Earth science: Investigations using remote sensing data, in Rencz, A.N., ed., Remote Sensing for the Earth Sciences: Manual of Remote Sensing, 3 ed., v. 3, New York, John Wiley, p. 251-306.

Phillips, C.H., Cornwall, H.R., and Rubin, M., 1971, A Holocene ore body of copper oxides and carbonates at Ray, Arizona: Economic Geology, v. 66, p. 495-498.

Phillips, C.H., Gambell, N.A., and Fountain, D.S., 1974, Hydrothermal alteration, mineralization, and zoning in the Ray deposit: Economic Geology, v. 69, p. 1237-1250.

Ransome, F.L., 1919, The copper deposits of Ray and Miami, Arizona: USGS, PP 115, 192 p. report with 1:125,000-scale geologic map (Plate II).

Sabine, C., 1999, Chapter 8 Remote sensing strategies for mineral exploration: in Rencz, A.N., ed., Remote Sensing for the Earth Sciences: Manual of Remote Sensing, 3 ed., v. 3, New York, NY, John Wiley & Sons, Inc., p. 375-447.

Sheskin, D.J., 1997, Handbook of parametric and nonparametric statistical procedures: CRC Press, Boca Raton, FL, p. 558-563.

Swayze, G.A., Clark, R.N., Smith, K.S., Hageman, P.L., Sutley, S.J., Pearson, RM., Rust, G.S., Briggs, P.H., Meier, A.L., Singleton, M.J., and Roth, S., 1998, Using imaging spectroscopy cost-effectively locate acid-generating minerals at mine site: an example from the California Gulch superfund site in Leadville, Colorado: Summaries of the Seventh JPL Airborne Earth Science Workshop Pasadena, JPL Pub. 97-21, v. 1, p. 385-389.

Tahl, S., and Schonermark, M.V., 1998, Determination of the column water vapour of the atmosphere using backscattered solar radiation measured by the Modular Optoelectronic Scanner (MOS): Intl. J. Remote Sensing, v. 19, n. 17, p. 3223-3236.

Wilson, E.D., Moore, R.T., Heindl, L.A., and Creasey, S.C., 1959, Geologic map of Pinal County, Arizona: University of Arizona, Arizona Bureau of Mines, 1:375,000-scale geologic map.

APPENDIX A

ANNOTATED LIST OF SOFTWARE, LIBRARY SPECTRAL DATA AND INSTRUMENTATION

Adobe Photoshop. We use this image editing, annotation and printing software package to create and print annotated AVIRIS images, to save AVIRIS image files in formats compatible with word processing programs, and to create image files for publication. Available commercially from Adobe Systems, Inc., San Jose, CA, http://www.adobe.com.

ASD. See text Table 1 for selected specifications. We used this field spectrometer (model FR) to measure reflectance spectra of the target. Available commercially from Analytical Spectral Devices, Inc., Boulder, CO, http://www.asd.com.

AVIRIS. See text Table 1 for selected specifications. We used the **A**irborne **V**isible and **I**nfrared **I**maging **S**pectrometer to image Ray Mine. Flown on an ER-2 aircraft at 20 km altitude and developed for NASA by JPL, this 224 channel imaging spectrometer is documented and image data are available from JPL, http://makalu.jpl.nasa.gov/ aviris.html.

Beckman. See text Table 1 for selected specifications. We used the Beckman (model UV5240) spectrometer for laboratory spectral measurements of rock samples collected in the field. Available commercially from Beckman Coulter, Inc., Fullerton, CA, http://www.beckman. com.

ENVI. We used this image processing software package, which is ideally suited to processing imaging spectrometry data, for opening and processing AVIRIS reflectance data, mapping mineralogy, extracting image spectra, and creating ASCII files

from AVIRIS pixel spectra. Includes the JPL spectral library. Available commercially from Research Systems, Boulder, CO, http://www.rsinc.com.

EXCEL. A robust spreadsheet and plotting program. Used to read spectral data files; edit bad/redundant channels; calculate reflectance, mean and 1 sigma spectra; calculate mean values, descriptive statistics, and confidence intervals; and plot spectra. Available commercially from Microsoft Corporation, Redmond, WA, http://www.microsoft.com.

Halon. A diffuse reflectance target used for converting Beckman laboratory spectra to absolute reflectance. The white powder that used is part no. 201365 available commercially from Diano Corporation, Woburn, MA, http://www.dianocorp.com/.

Library Spectra. Reflectance spectra for minerals from the JPL spectral library were used to aid interpretation and analysis of laboratory, field and AVIRIS reflectance spectra. This library is included in the ENVI software package and in the ASTER spectral library available from JPL, Pasadena, CA, http://speclib.jpl.nasa.gov/.

MODTRAN. The **MOD**erate Resolution **TRAN**smittance code, a robust, validated and well documented radiative transfer model. Used in the Green et al. (1996 and 1998) method to convert calibrated AVIRIS radiance data to reflectance. Developed at Hanscom AFB, MA, the code can be downloaded from http://www-vsbm.plh.af.mil/.

Omnistar. We used this satellite broadcast, real-time differential correction system with our Trimble GPS receiver to obtain accurate locations for our field station.

Available commercially from Omnistar, Inc., Houston, TX, http://www.omnistar.com.

PIMA. See text Table 1 for selected specifications. A field spectrometer that we used in the laboratory for spectral measurements of samples collected in the field. Available commercially from Spectral International, Inc., Arvada, CO, http://www.pimausa.com.

Spectralon. Diffuse reflectance target. Provides a standard for converting ASD field spectra to absolute reflectance. The 5" x 5" calibration plate that we used is part no. SRT-99-050 available commercially from Labsphere, Inc., North Sutton, NH, http://www.lapsphere.com/stan8.htm.

Trimble. A global positioning system (GPS) receiver equipped to receive Omnistar real-time differential corrections. We used a model TDC2 instrument to obtain better-than 5 m (x,y,z) accuracy locations for field stations. Available commercially from Trimble Navigation Limited, Sunnyvale, CA, http://www. trimble.com.

XRD. X-Ray Diffraction, a standard laboratory procedure used for determining mineralogy of geological samples. We used a Philips Analytical, Type 42273, powder diffractometer instrument with a Cu X-ray source, powered at 40 kV and 20 Ma to determine the mineralogy of samples from the target surface. Data were collected every 0.02° 2Theta with 1 second counting time. The system is modified for computer control and has upgraded optics, a new digital detection system and an automated slit width control. Available commercially from Philips Analytical, Mahwah, NJ, http://www-eu.analytical.philips.com/wwa/usa1.stm.

Xyez. A robust plotting program used to plot spectra, calculate spectra of mixtures of library mineral spectra, and measure wavelength positions of features on reflectance spectra. Available commercially from Stanage Edge Software, Altadena, CA, http://www.xyez.com.

TABLES

Table 1. Specifications of spectrometers used for validation. Nominal spectral resolution, a function of channel width and sampling interval, is at 2.2 μm.

SPECTROMETER	FIELD OF VIEW		RANGE (μm)	RESOLUTION (μm)
	R (cm)*	AREA (cm^2)		
Beckman	1.15	4.2	0.40-2.50	0.004
PIMA	0.50	0.8	1.30-2.50	0.002
ASD	6.99**	153.5	0.35-2.50	0.005
AVIRIS	2000***	4,000,000	0.40-2.50	0.010

* R is radius of sample surface measured.
** With 8° optical head at 1 m from measurement surface.
*** Pixel size for measurements from ER-2 aircraft at 20 km altitude above terrain.

Table 2. Summary of spectral absorption band positions (in μm) that we identified in qualitative assessment of upper tier reflectance spectra. Bands that are aligned in the same column are those that are coincident in wavelength when the spectral resolutions of the instruments (Table 1) are considered.

LIBRARY MINERAL SPECTRA (Figure 5)											
Quartz											
Kaolinite				0.96	1.23	1.30		2.16	2.20	2.32	2.38
Plagioclase					1.27				2.19	2.32	
Jarosite	0.44	0.57		0.91					2.27		
Muscovite				0.92			2.10		2.19	2.35	
Goethite	0.41	0.48	0.65	0.90					2.20		
Hematite		0.51	0.67	0.87							
CALCULATED LIBRARY MINERAL MIXTURE SPECTRA (Figure 6)											
Mixtures 1&2		0.51	0.65	0.90					2.19	2.33	
LABORATORY ROCK SPECTRA (Figure 7 and 8)											
Beckman		0.52	0.67	0.87			2.10	2.16	2.20	2.32	
PIMA----------N/A----------							2.10	2.16	2.20	2.33	
FIELD SPECTRA (Figure 9)											
ASD		0.52	0.67	0.87			2.10		2.20	2.34	
IMAGE SPECTRA (Figure 10)											
AVIRIS		0.53	0.67	0.87			2.10		2.19	2.34	

Table 3. Mean reflectance (and 1 sigma) at wavelengths corresponding to reflectance peaks exhibited by upper-tier validation target spectra illustrated in Figures 6, 7, 8, 9, and 10.

	REFLECTANCE (%) AT REFLECTANCE PEAK		
	0.78 µm	**1.60 µm**	**2.27 µm**
Library Mixture Spectra	42-46	51-54	44-49
Beckman	33 (10)	49 (10)	35 (9)
PIMA	N/A	35 (7)	23 (6)
ASD	28 (4)	44 (6)	30 (4)
AVIRIS	31 (1)	53 (1)	33 (1)

Table 4. AVIRIS image/ASD field spectra comparison for 15 stations on traverse A.

BR/BD (μm)*	Mean bias (Rel %)	RSD% ASD means	RSD% AVIRIS
0.86/0.73	3.1/1.6	2.9/1.0	1.5/0.8
0.86/1.60	6.6/4.3	9.9/6.5	5.7/3.8
2.20/1.60	7.8/5.2	5.4/3.6	2.2/1.5
2.20/2.27	1.0/0.6	3.1/1.8	2.7/1.6
2.16/1.60	11.2/7.0	5.7/3.4	2.5/1.6
2.20/2.16	-4.1/(-2.3)	6.4/3.7	3.3/1.8
2.16/2.20 (ASR)	-15.8	11.1	4.1

* See text for algorithms for band ratio (BR), band depth (BD), and absorption slope ratio (ASR). Reference reflectance for ASR (U in equation 3) was at 1.60 μm.

Table 5. AVIRIS image/ASD field spectra comparison for 15 stations on traverse A.

BR (μm)*	Sys behav? ASD means	Sys behav? AVIRIS	Pearson** r ASD means	Pearson r AVIRIS	Z***	Sig diff?
0.86/0.73	y	y	-0.75	-0.77	0.12	n
0.86/1.60	y	y	-0.75	-0.78	0.18	n
2.20/1.60	n	n	0.27	0.14	0.33	n
2.20/2.27	n	n	0.34	0.32	0.05	n
2.16/1.60	y	y	-0.67	-0.66	-0.04	n
2.20/2.16	y	y	0.70	0.62	0.35	n
2.16/2.20 (**ASR**)	y	y	0.72	0.67	0.24	n

* See text for algorithms for band ratio (BR) and absorption slope ratio (ASR).

** Only BR and the ASR values are shown for brevity. Conclusions are the same for the BD. The test appears in Sheskin (1997).

*** See text for definition of test statistic and critical region.

FIGURE CAPTIONS

Figure 1. Location of Ray Mine in central southeastern Arizona. Small map of the state of Arizona shows area covered by the large map. Superior, Miami, Globe, Winkelman and Christmas are other mine sites in the vicinity of Ray Mine.

Figure 2. A. 1997 AVIRIS color composite image of the Ray Mine area. In this color infrared rendition, vegetation appears in tones of red. Blue and white areas are devoid of vegetation, and black areas are water or dark shadows. B. Simplified geologic map of the area covered by A. (After Ransome, 1919, and Creasey et al., 1983).

Figure 3. Color composite image of the validation target extracted from Figure 2. A. Also shown is the location of transect A. Stations 1 through 6 are on the upper tier and stations 7 through 15 are on the lower tier of the target.

Figure 4. June, 1998, field photographs of the validation target. Clockwise from top left: ASD field spectrometer set-up showing shoulder-hung laptop computer, optical head mounted on end of 1 m stick, and Spectralon calibration plate mounted horizontally on tripod; view to the SW showing typical upper tier target surface in the foreground, and typical vegetation and terrain outside the area of mining operations in the background; view to the NE showing typical upper tier target surface in the foreground and typical area of mining operations in the background; view to the SE

showing typical lower tier target surface in the foreground and typical slope on the edge of the upper tier target surface in the background.

Figure 5. Beckman library spectra of 7 minerals identified in rock samples collected randomly on the upper tier of the validation target (from Grove et al., 1992): red, kaolinite; orange, quartz; light blue, plagioclase; green, muscovite; dark blue, jarosite; greenish gray, goethite; and violet, hematite. Wavelengths blocked out by the gray rectangles are those unavailable in AVIRIS spectra because of the effects of atmospheric water absorption.

Figure 6. Spectra calculated by linear mixing of spectra for selected minerals from Figure 5. Green spectrum: 36% goethite, 29% muscovite, 21% hematite, and 14% kaolinite. Blue spectrum: 20% goethite, 30% muscovite, 30% hematite, 10% kaolinite, and 10% jarosite.

Figure 7. Mean (red), mean + 1 standard deviation (blue), mean - 1 standard deviation (orange), and 1 standard deviation (green) spectra from 32 Beckman laboratory spectra measured on the surfaces of 24 rock samples collected randomly on the upper tier of the validation target.

Figure 8. Mean (red), mean + 1 standard deviation (blue), mean - 1 standard deviation (orange), and 1 standard deviation (green) spectra from 32 PIMA laboratory

spectra measured on the surfaces of 24 rock samples collected randomly on the upper tier of the validation target.

Figure 9. Mean (red), mean + 1 standard deviation (blue), mean - 1 standard deviation (orange), and 1 standard deviation (green) spectra from 60 ASD field spectra measured on the upper tier of the validation target where samples for the Figure 7 and 8 spectra were collected.

Figure 10. Mean (red), mean + 1 standard deviation (blue), mean - 1 standard deviation (orange), and 1 standard deviation (green) spectra from six AVIRIS spectra measured on the upper tier of the validation target where spectra for Figure 9 were measured.

Figure 11. Plot showing 0.86/1.60 μm band ratios from ASD mean and corresponding AVIRIS reflectance spectra along transect A (Figure 3). The 95% confidence intervals on local ASD mean values are also shown. Note similar decreasing tendencies of both ASD and AVIRTIS band ratios along the transect.

Figure 12. AVIRIS and mean ASD spectra with 2 sigma limits for station 1. This mean ASD spectrum produced the maximum values for any station for band ratio 0.86/0.73 μm and the ASR.

Figure 13. AVIRIS and mean ASD spectra with 2 sigma limits for station 2. This mean ASD spectrum produced the maximum values for any station for band ratio 2.16/1.60 μm.

Figure 14. AVIRIS and mean ASD spectra with 2 sigma limits for station 3. This mean ASD spectrum produced the maximum value for any station for band ratio 2.20/2.16 μm and the minimum values for 0.86/0.73 μm and the ASR.

Figure 15. AVIRIS and mean ASD spectra with 2 sigma limits for station 5. This mean ASD spectrum produced the maximum value for any station for 0.86/1.60 μm and the minimum values for 2.20/1.60, 2.20/2.27 μm and 2.20/2.16 μm.

Figure 16. AVIRIS and mean ASD spectra with 2 sigma limits for station 7. This mean ASD spectrum produced the maximum values for any station for band ratio 2.20/1.60 μm and 2.20/2.27 μm.

Figure 17. AVIRIS and mean ASD spectra with 2 sigma limits for station 14. This mean ASD spectrum produced the maximum value for any station for band ratio 0.86/1.60 μm.

Figure 18. AVIRIS and mean ASD spectra with 2 sigma limits for station 15. This mean ASD spectrum produced the maximum value for any station for band ratio 2.16/1.60 μm.

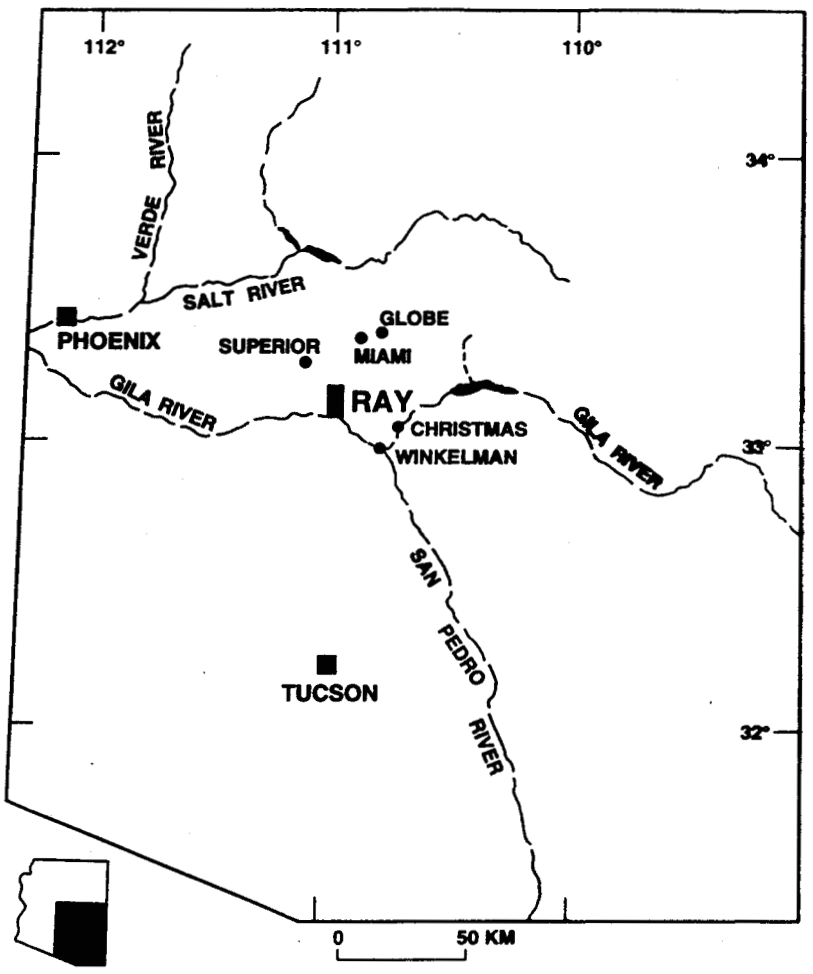

Fig. 1 Lang & Balogh

Fig. 2A
Leung & Baluga

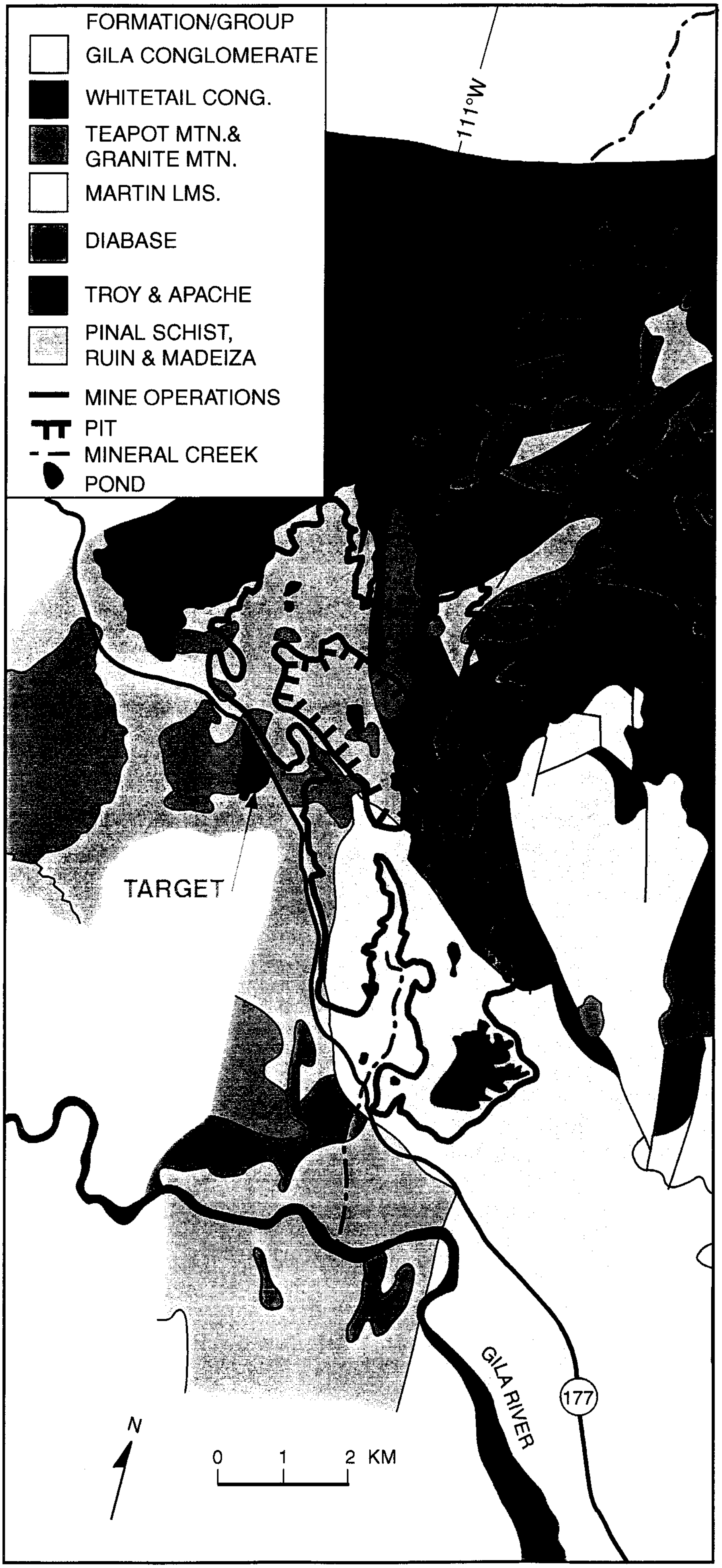

Fig. 2B
Lang & Eaton

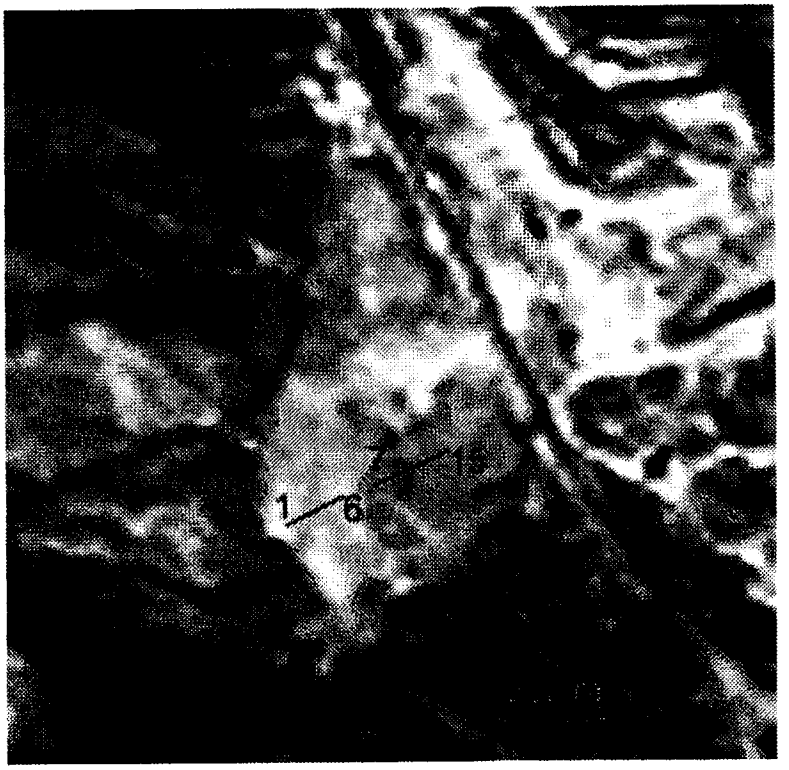

Fig. 3
LANG & BALOGA

FIG 4 LANG & BALCOA

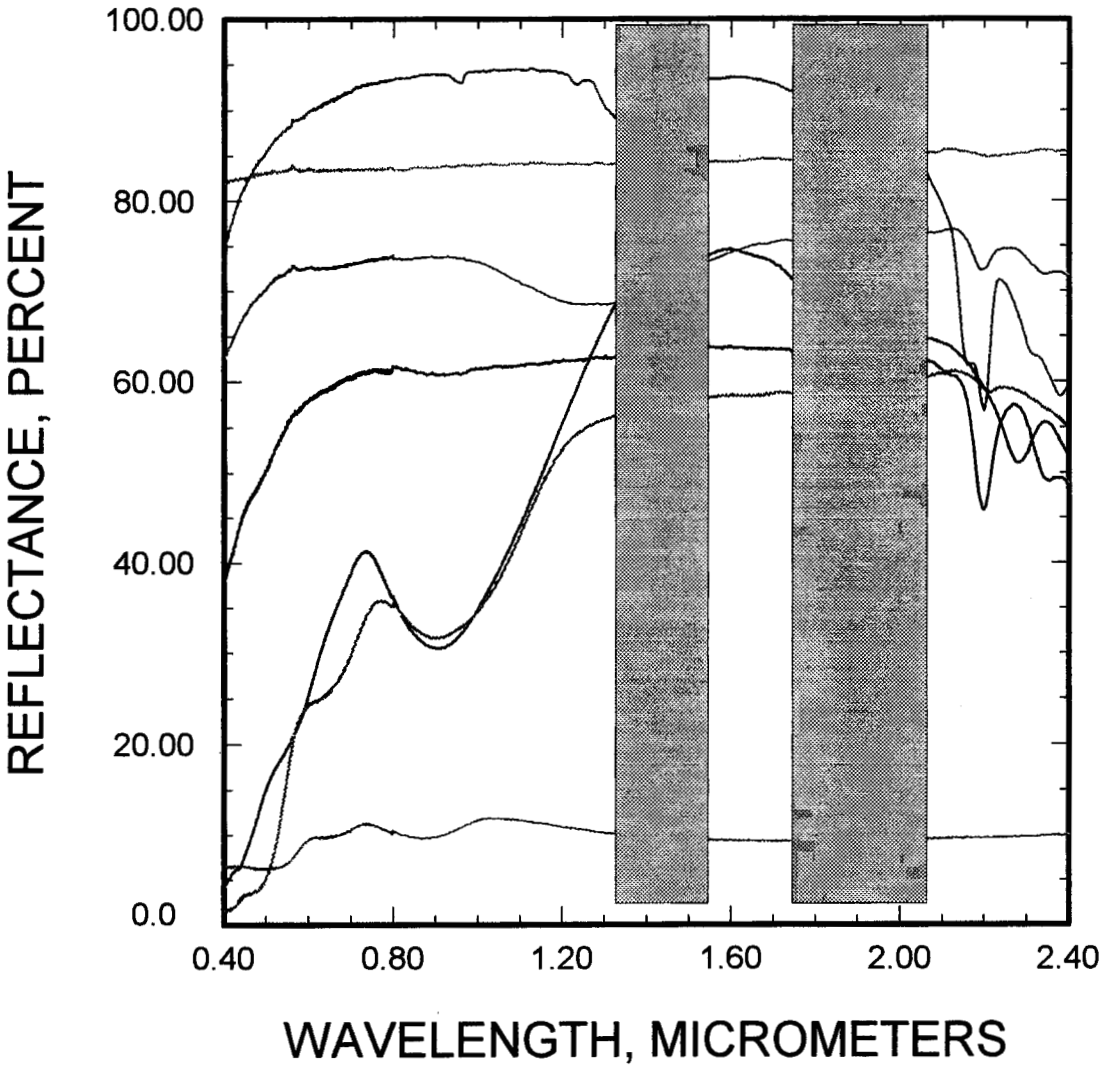

FIG. 5
LANG & BALOGA

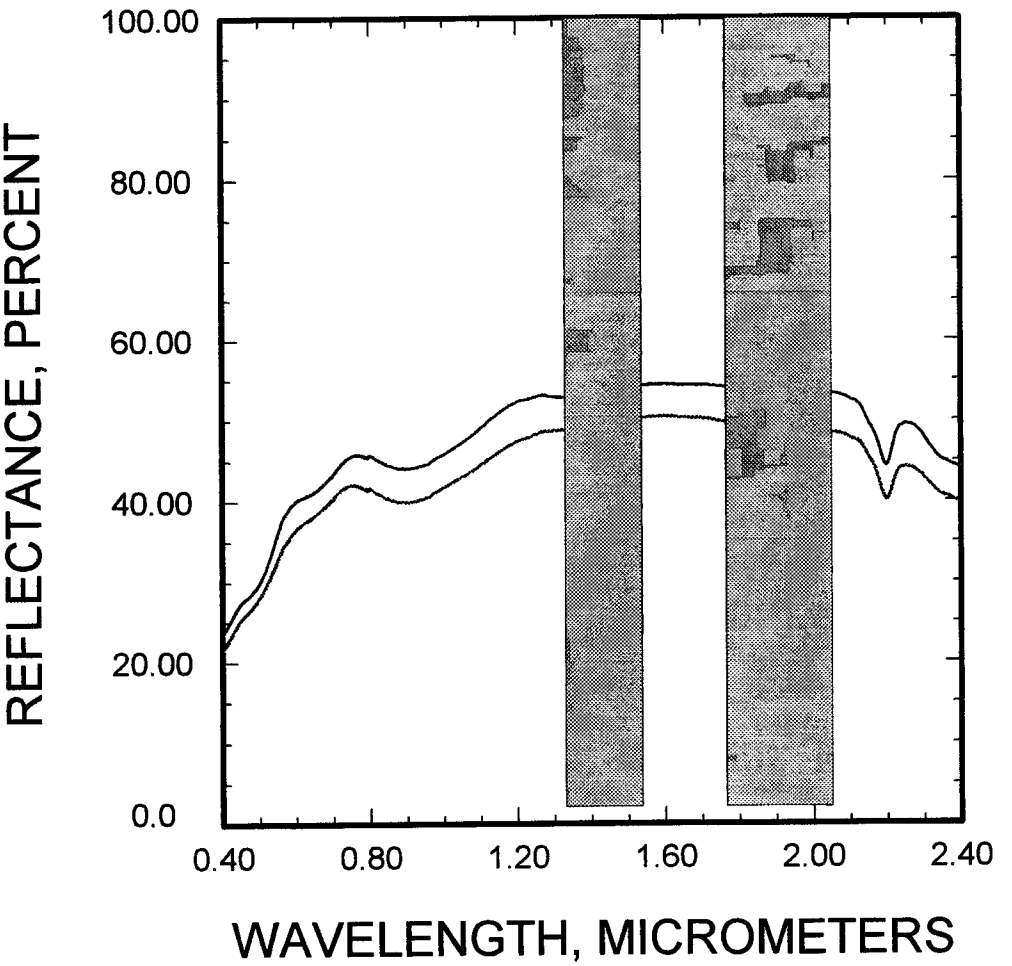

Fig. 6 Lang & Baloga

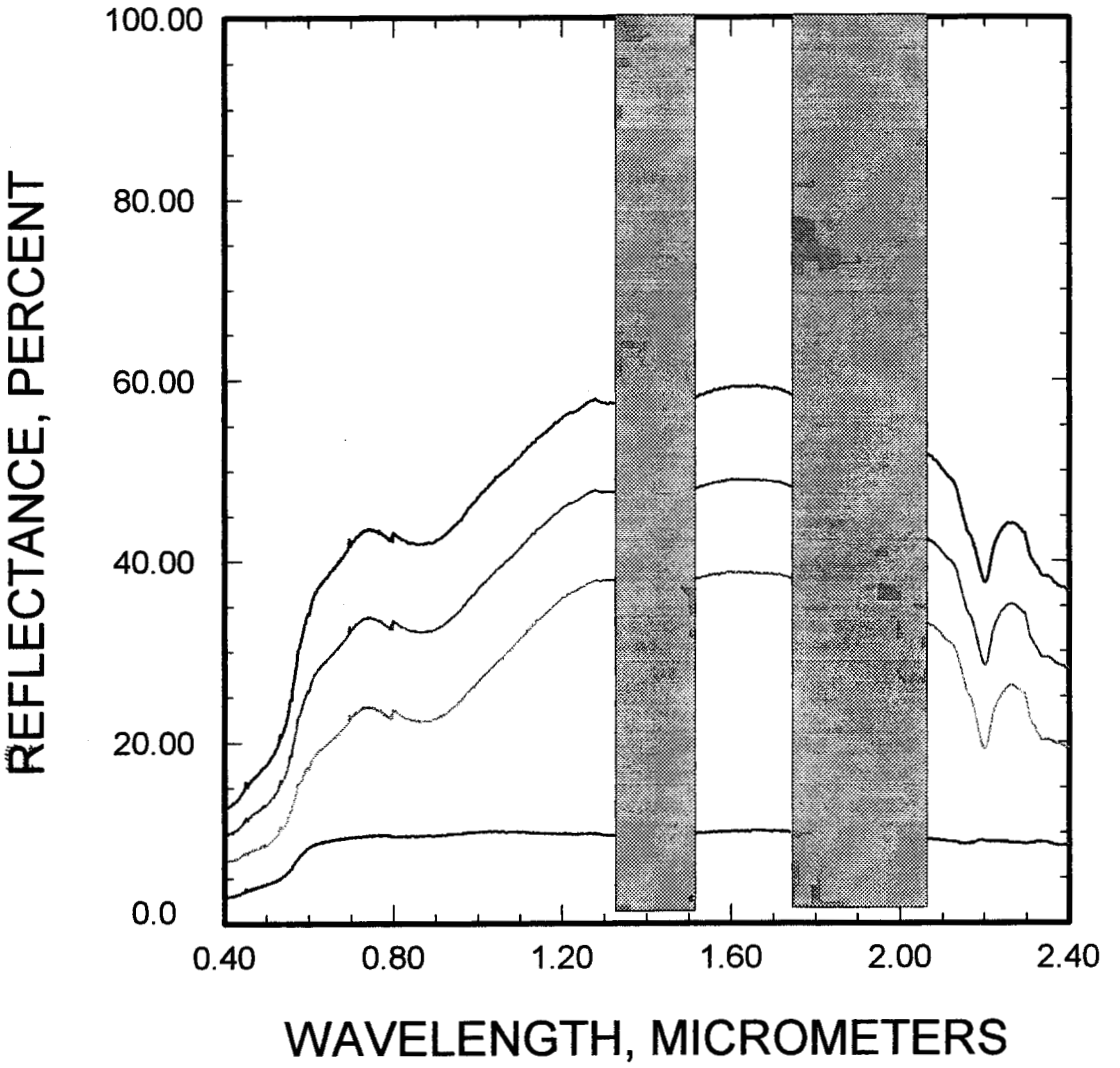

Fig 7. Lang & Baloga

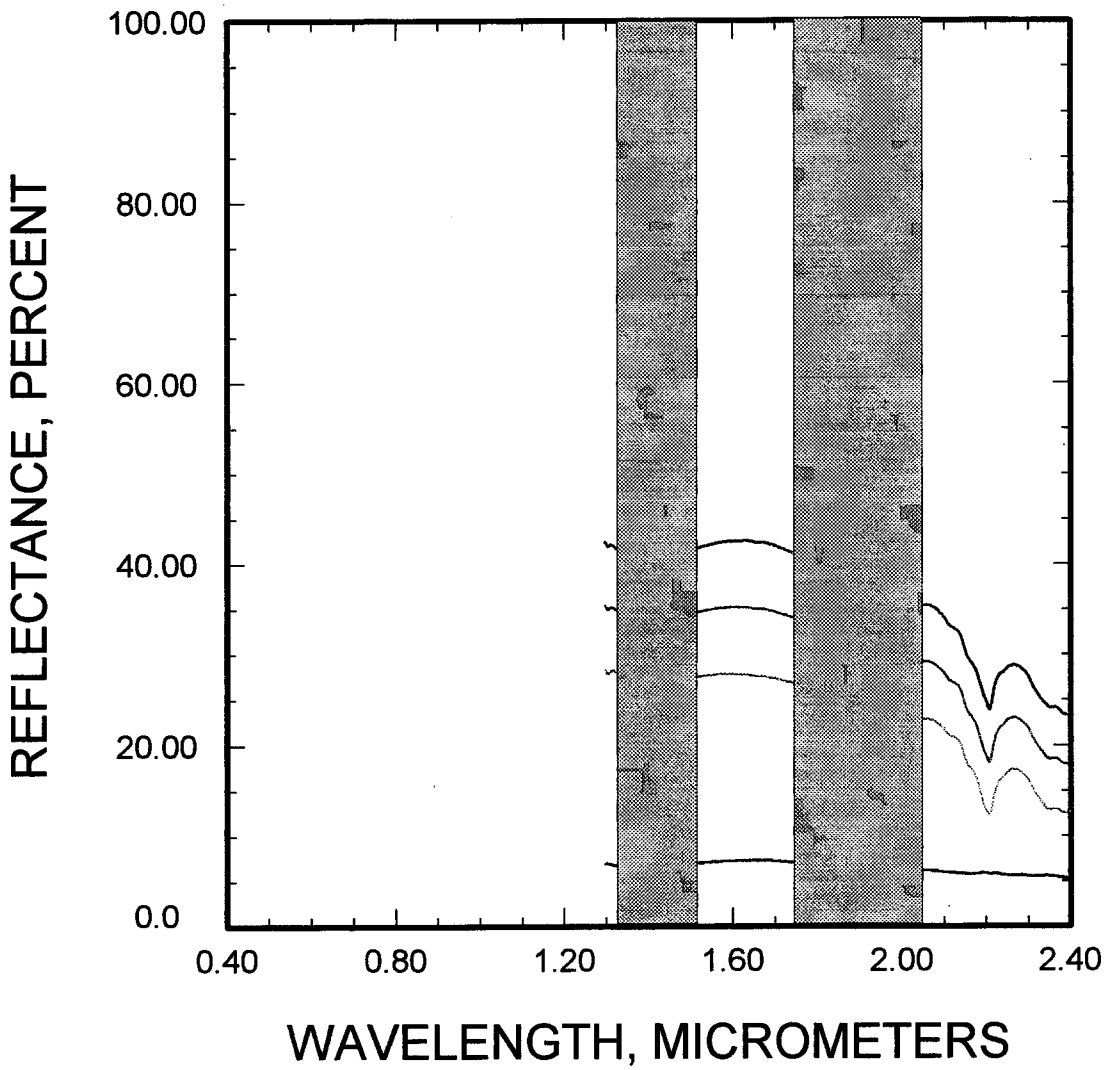

Fig. 8 Lang & Baloga

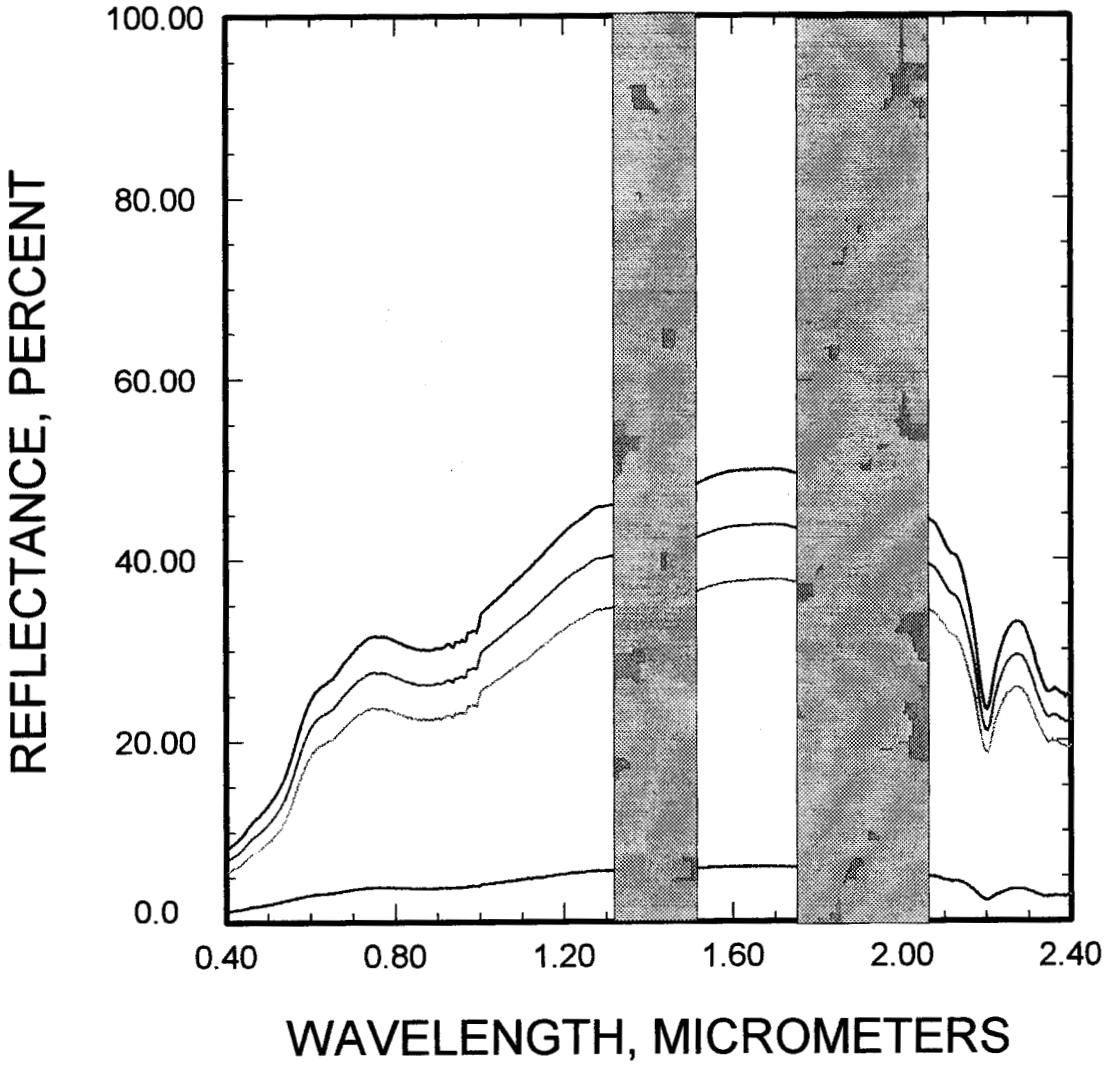

Fig. 9 Lang & Baloga

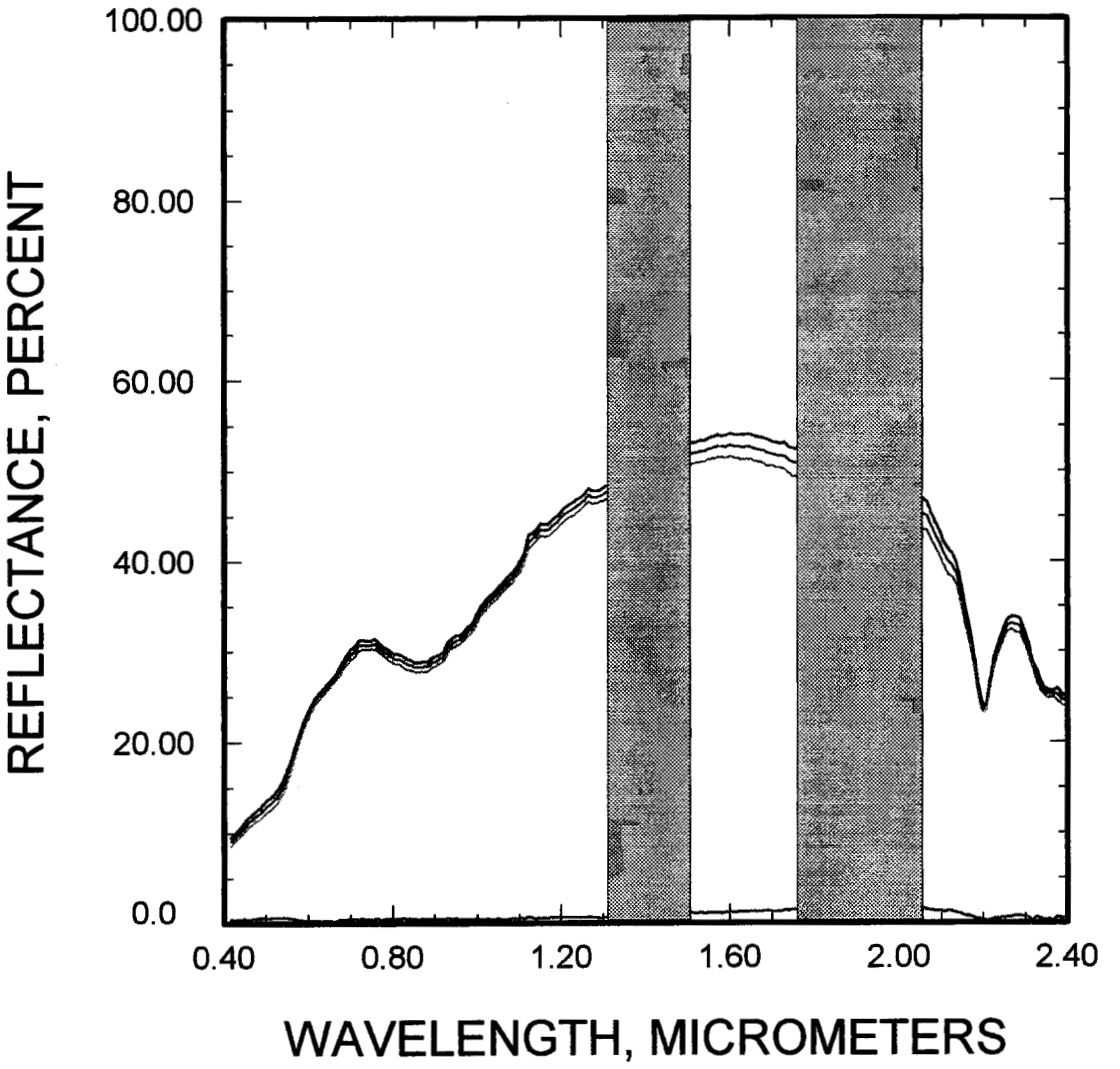

Figure 10, Lang & Baloga

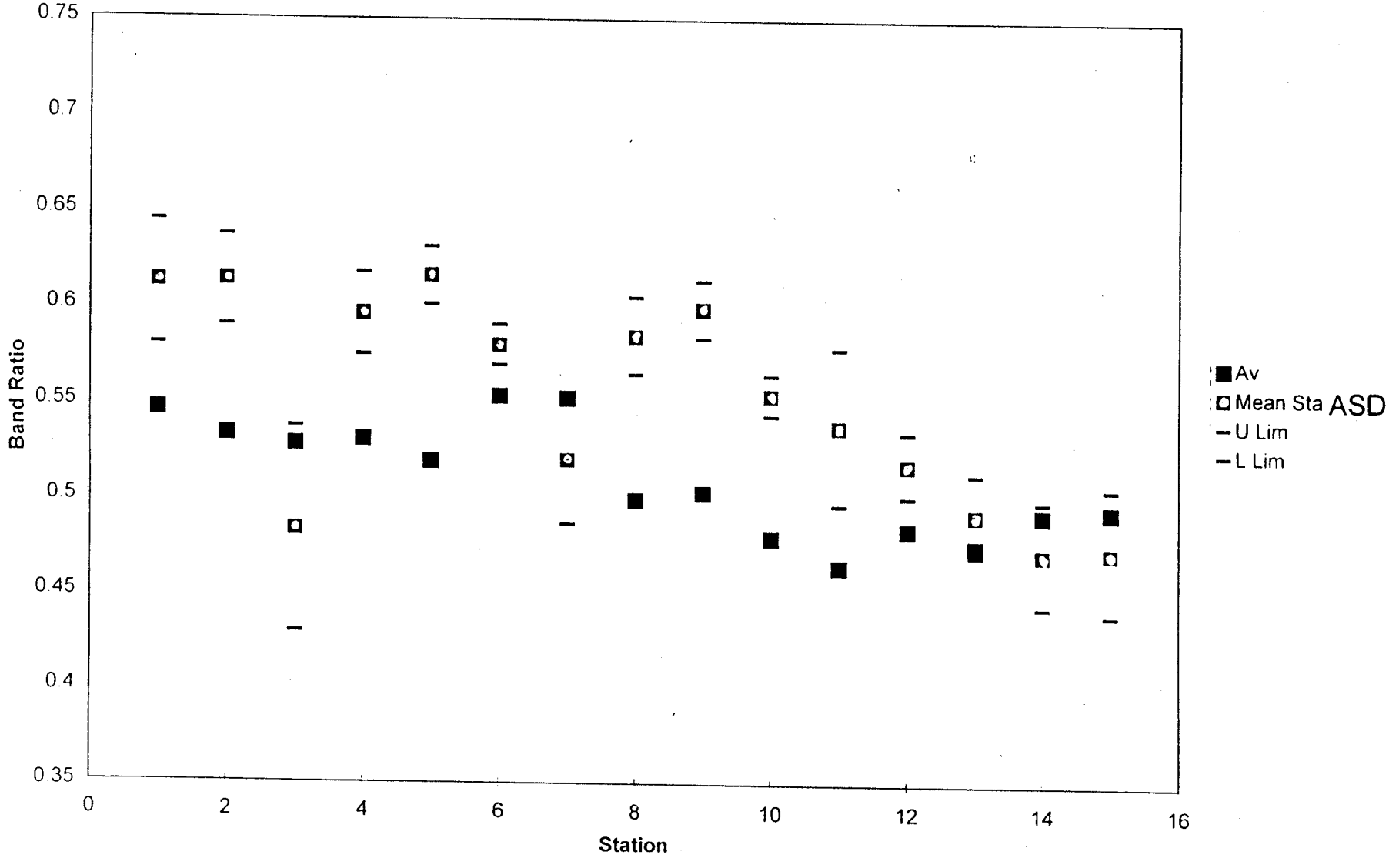

Fig 11 Lang & Baloga

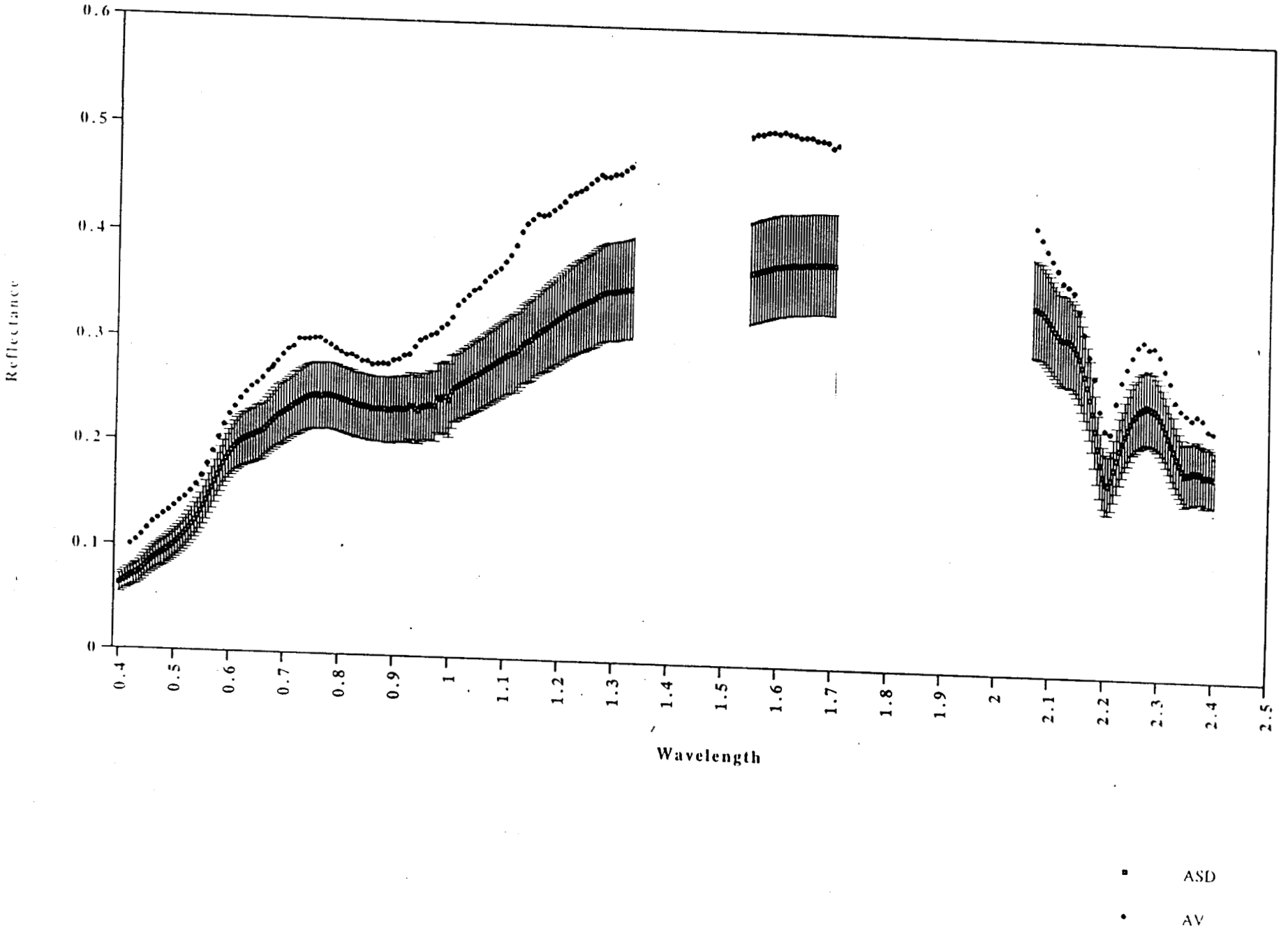

Fig 12 LANDSAT of Bologa

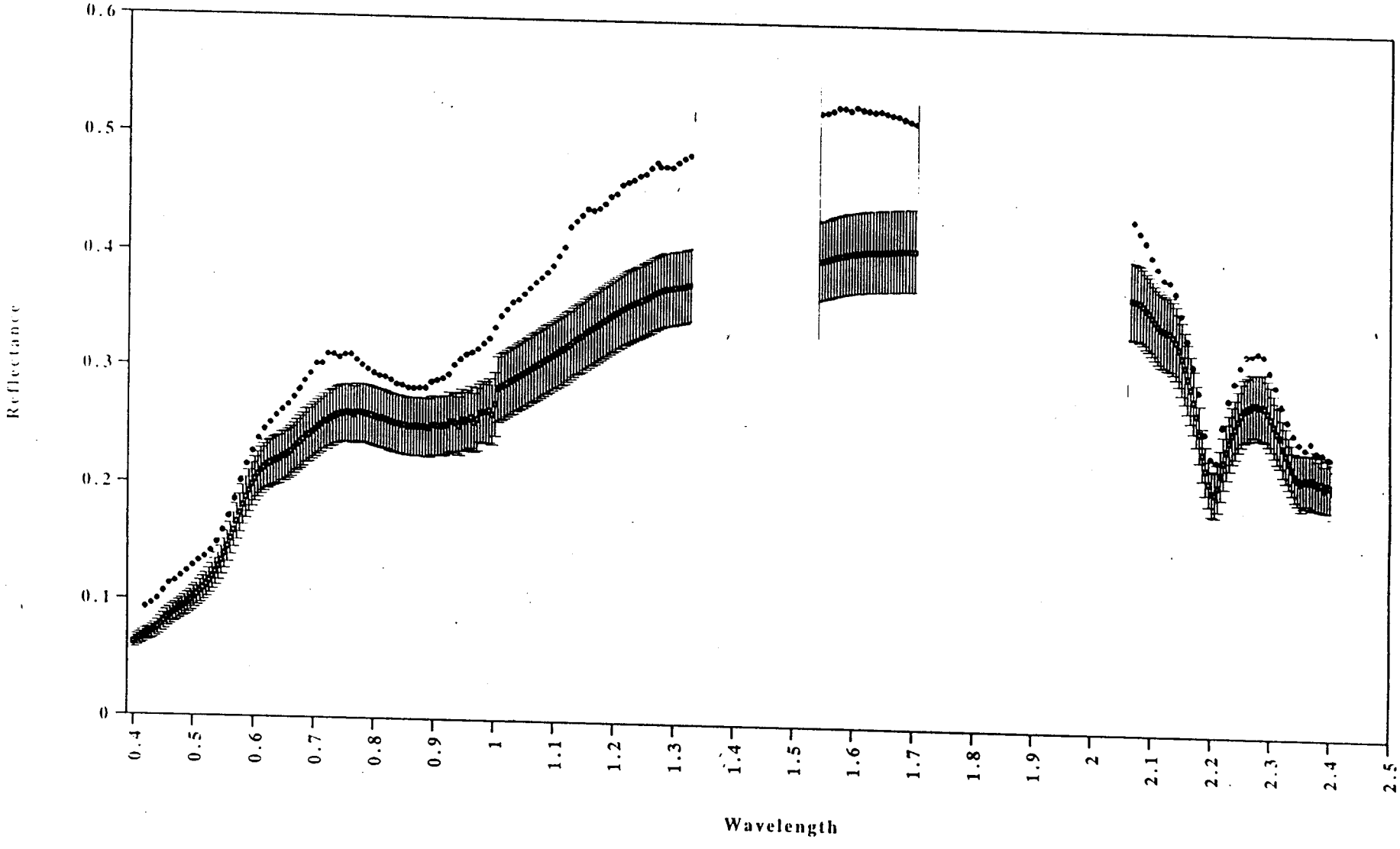

Fig 13 Lang & Baloga

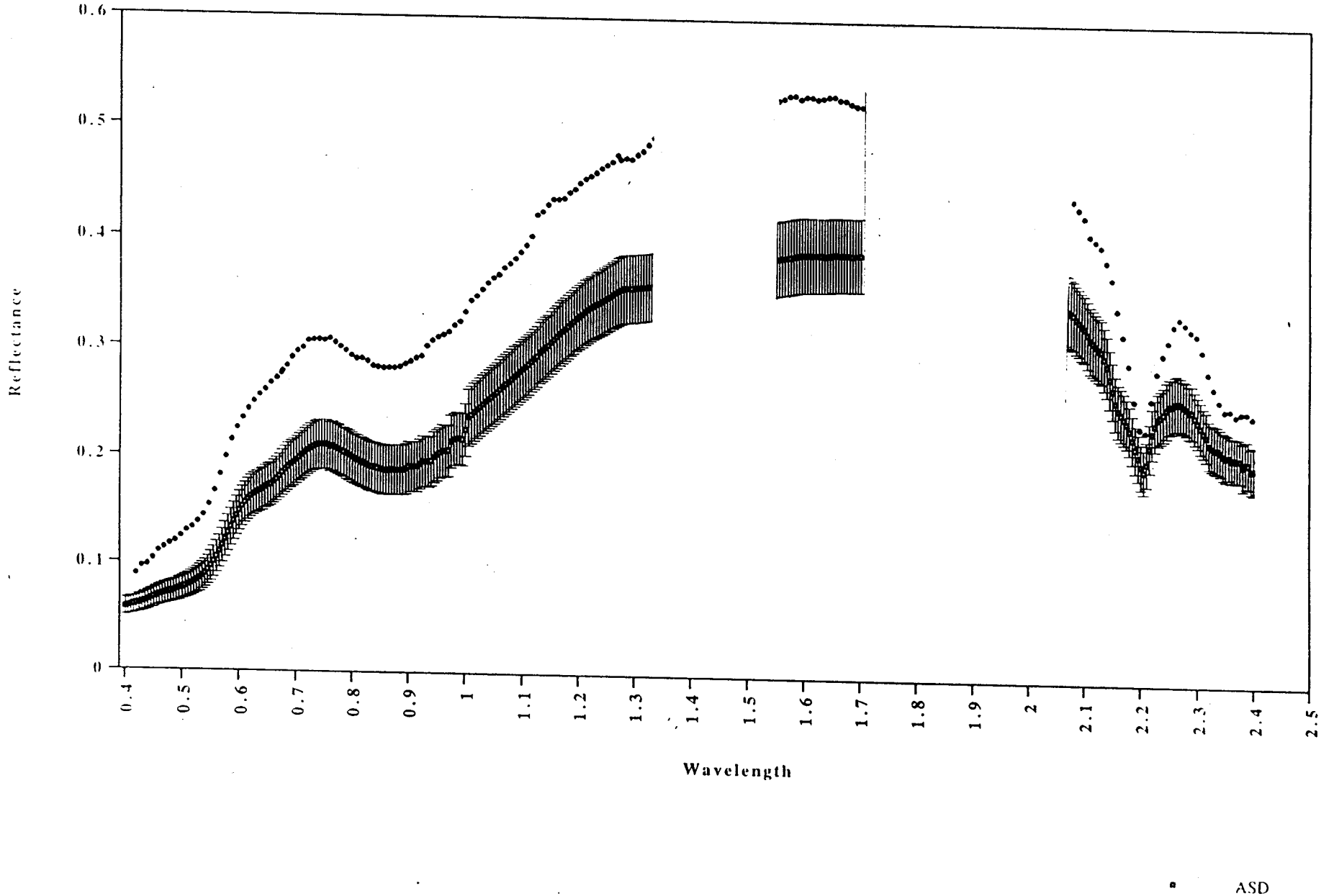

Fig 14 Lang & Baloga

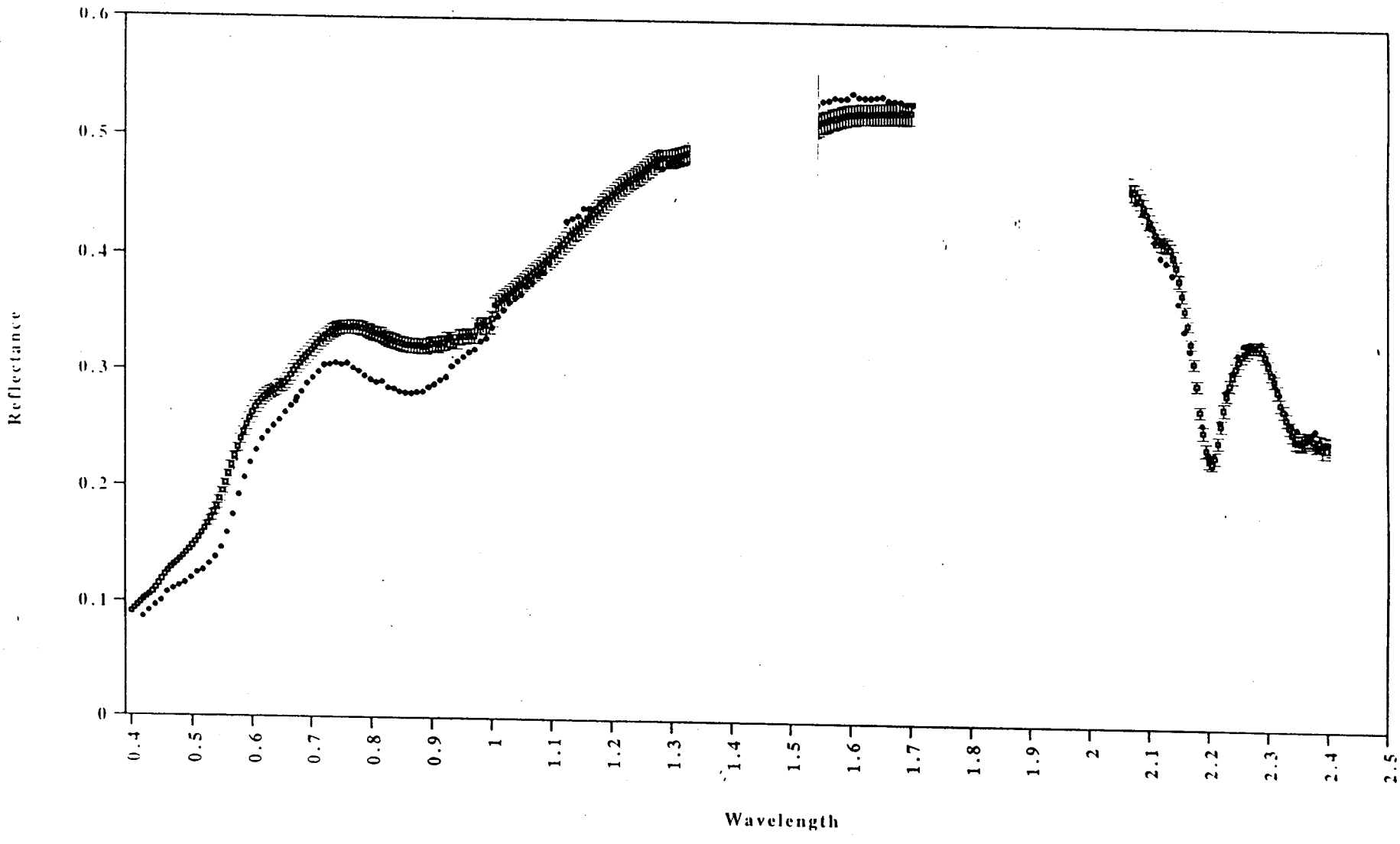

Fig 15 Lang & Baloga

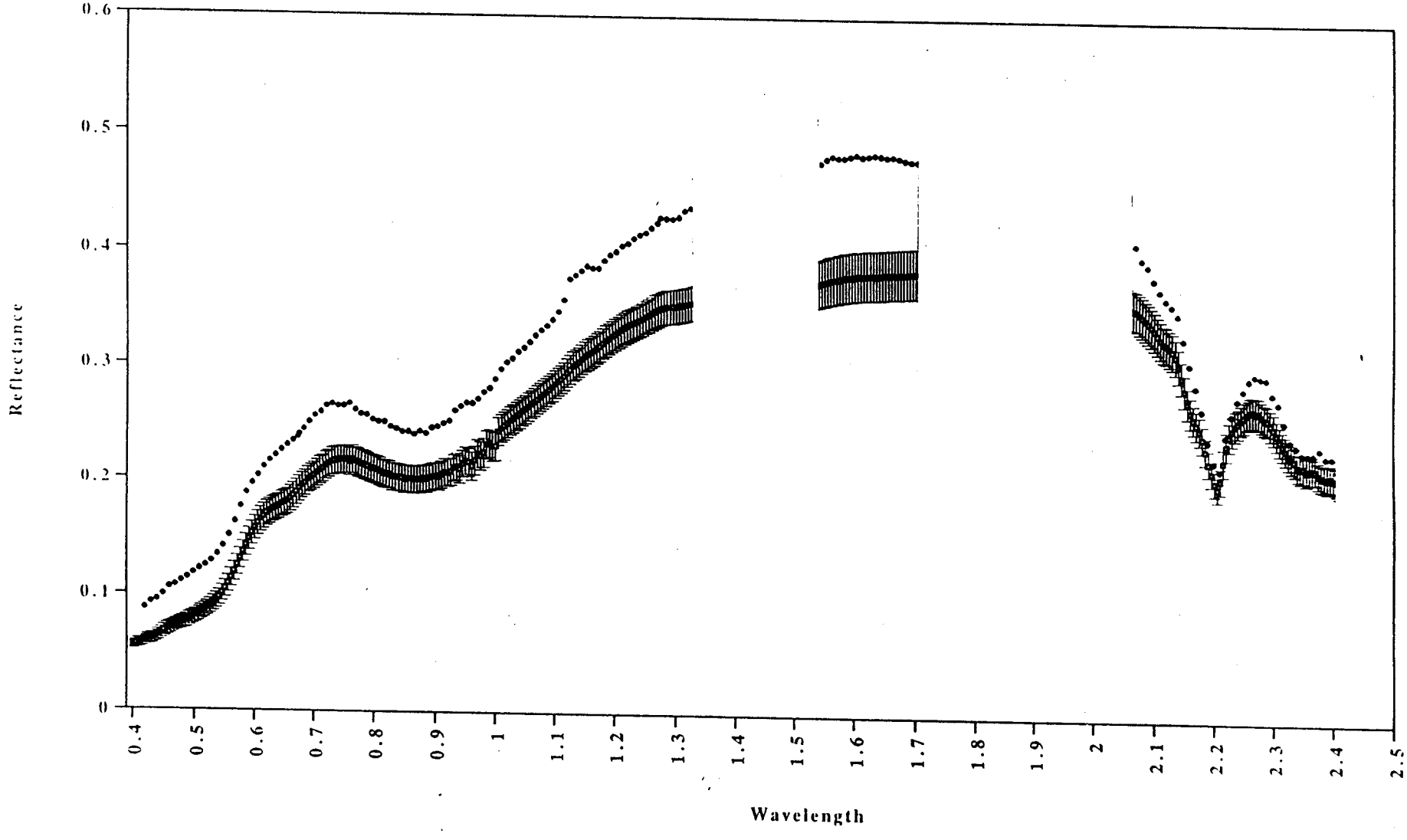

Fig 16 Lang & Baloga

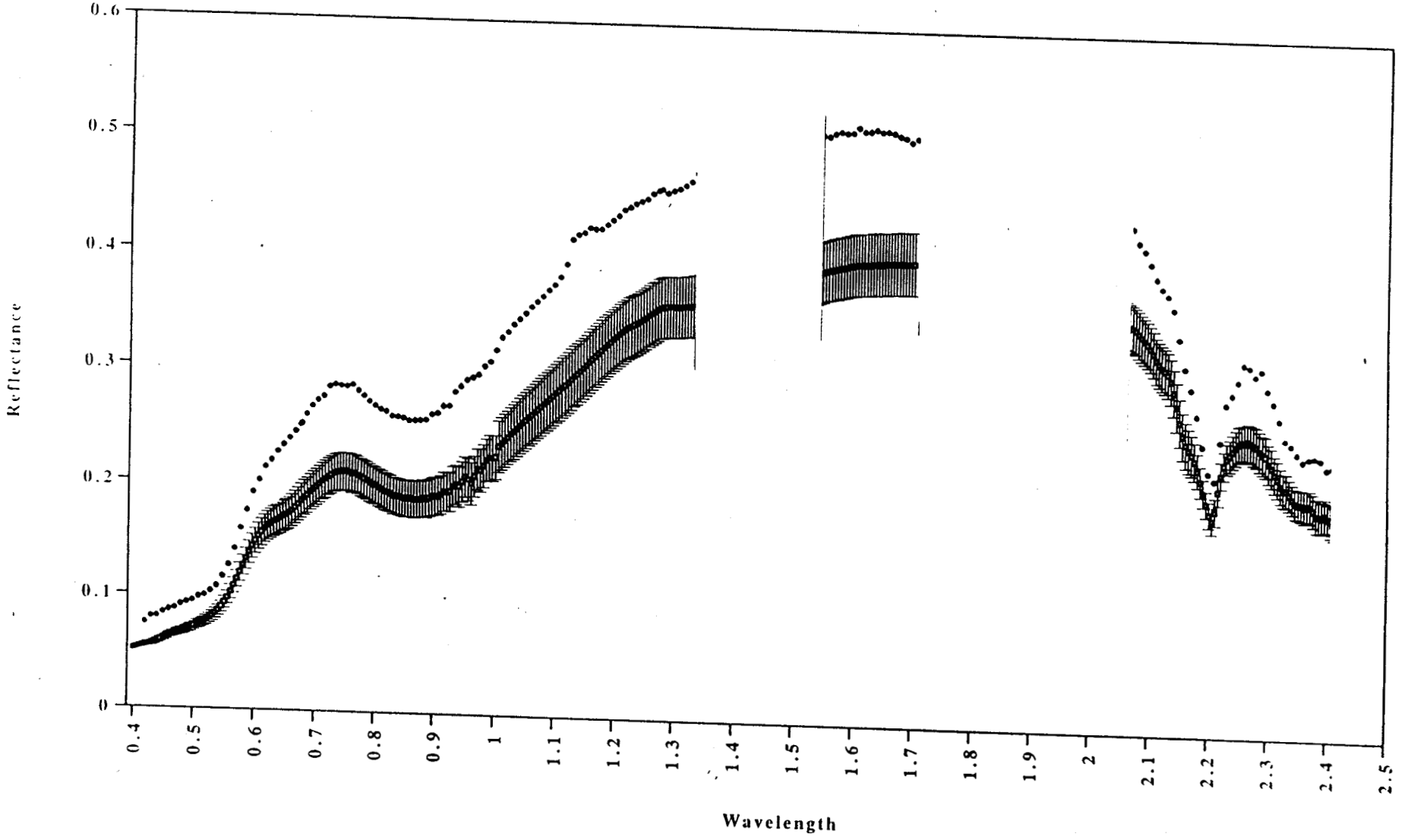

Fig 17 Lang & Baloga

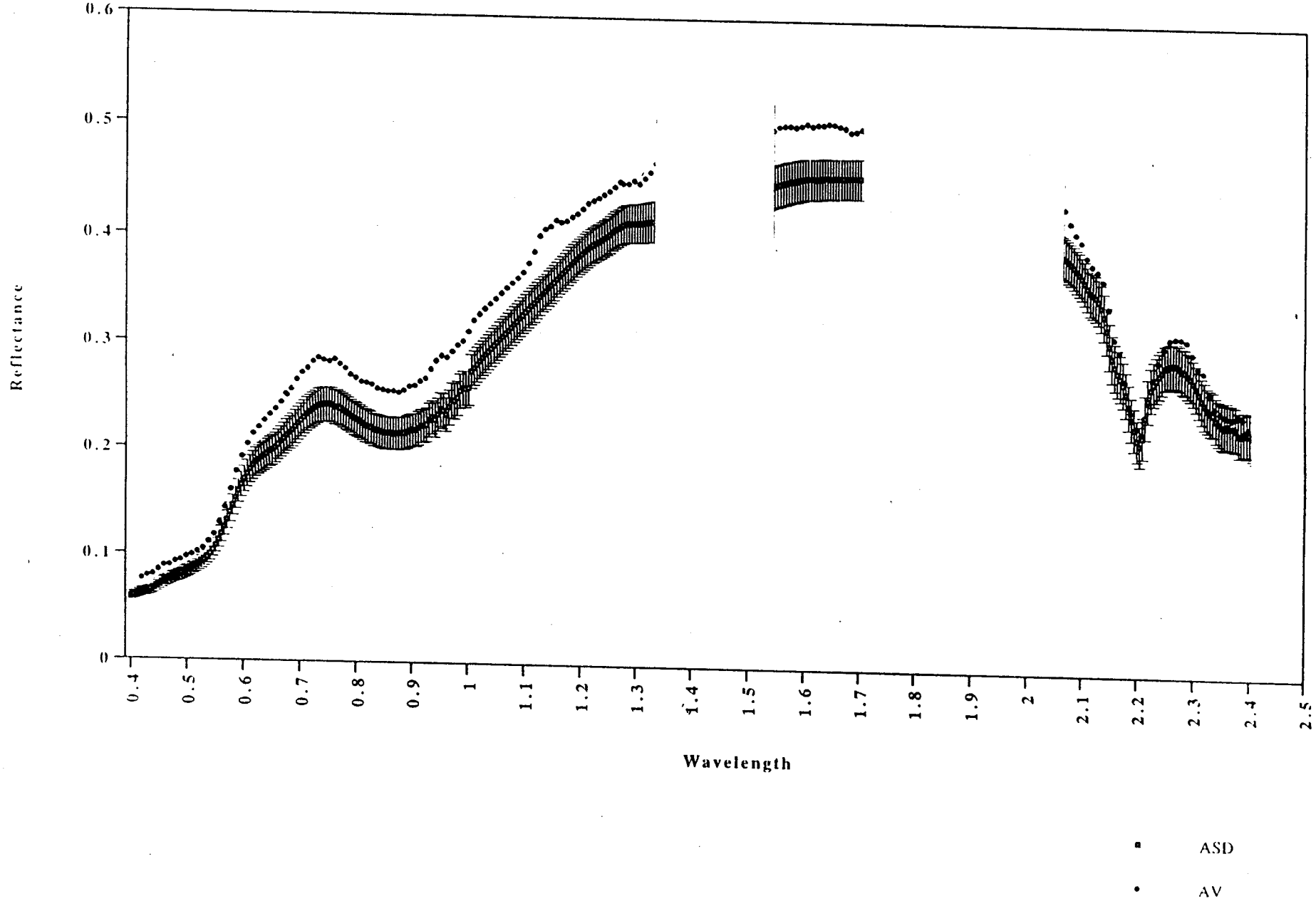

Fig 18. Lang & Baloga